HHS Public Access

Author manuscript

Cell. Author manuscript; available in PMC 2023 March 03.

Published in final edited form as:

Cell. 2022 March 03; 185(5): 815–830.e19. doi:10.1016/j.cell.2022.01.010.

GPR35 promotes neutrophil recruitment in response to serotonin metabolite 5-HIAA

Marco De Giovanni[1,*], **Hanson Tam**[1], **Colin Valet**[2], **Ying Xu**[1], **Mark R. Looney**[2], **Jason G. Cyster**[1,*,3]

[1]Howard Hughes Medical Institute and Department of Microbiology and Immunology, University of California, San Francisco, San Francisco, CA 94143, USA.

[2]Departments of Medicine and Laboratory Medicine, University of California, San Francisco, San Francisco, 94143, CA, USA.

[3]Lead Contact

SUMMARY

Rapid neutrophil recruitment to sites of inflammation is crucial for innate immune responses. Here we reveal that the G-protein coupled receptor GPR35 is upregulated in activated neutrophils, and it promotes their migration. GPR35-deficient neutrophils are less recruited from blood vessels into inflamed tissue and the mice are less efficient in clearing peritoneal bacteria. Using a bioassay, we find that serum and activated platelet supernatant stimulate GPR35 and we identify the platelet-derived serotonin metabolite 5-hydroxyindoleacetic acid (5-HIAA) as a GPR35 ligand. GPR35 function in neutrophil recruitment is strongly dependent on platelets with the receptor promoting transmigration across platelet-coated endothelium. Mast cells also attract $GPR35^{+}$ cells via 5-HIAA. Mice deficient in 5-HIAA show a loss of GPR35-mediated neutrophil recruitment to inflamed tissue. These findings identify 5-HIAA as a GPR35 ligand and neutrophil chemoattractant and establish a role for platelet- and mast cell-produced 5-HIAA in cell recruitment to sites of inflammation and bacterial clearance.

In brief

Platelet- and mast cell-derived 5-HIAA is a ligand of GPR35 that promotes neutrophil transedothelial migration and recruitment to sites of inflammation upon bacterial infection

Graphical Abstract

*Correspondence: Marco.DeGiovanni@ucsf.edu (MD) and Jason.Cyster@ucsf.edu (JGC).

Author Contributions

M.D and J.G.C. conceptualized the study, designed the experiments, analyzed the data and wrote the manuscript. M.D. performed most experiments. H.T and Y.X. performed in vitro assays and provided input on the manuscript. C.V. and M.R.L. purified / activated platelets and provided critical reagents and expertise.

Declaration of interest

The authors declare no competing interests.

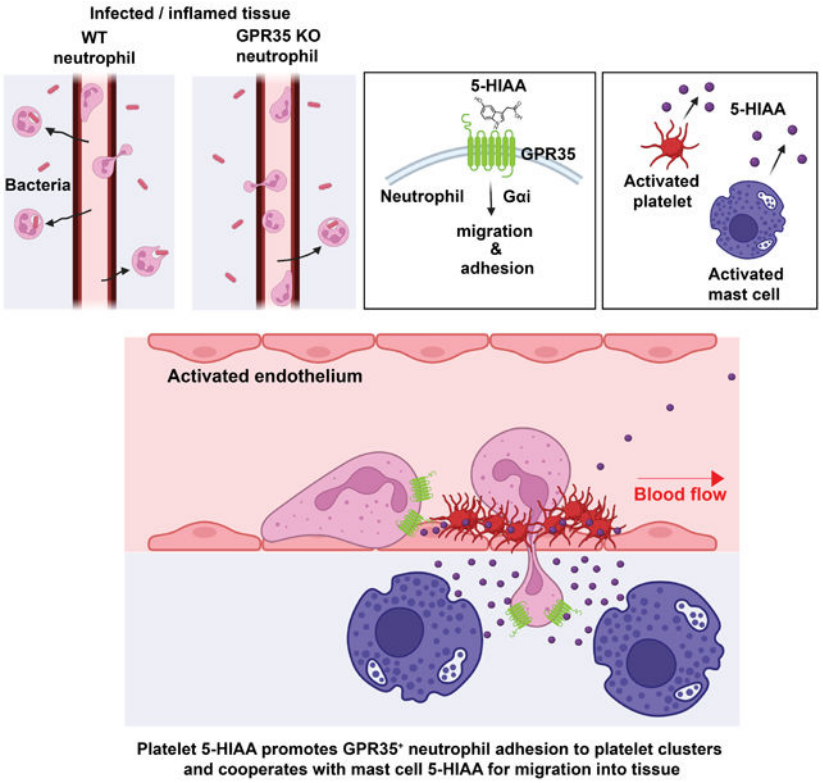

Platelet 5-HIAA promotes GPR35^{+} neutrophil adhesion to platelet clusters and cooperates with mast cell 5-HIAA for migration into tissue

INTRODUCTION

Neutrophils are crucial early responders at sites of inflammation, mediating rapid clearance of invading bacteria, and defects in neutrophil recruitment are a cause of recurrent infections in humans (Etzioni, 2009). Neutrophil recruitment to sites of inflammation occurs via a multistep cascade (Nourshargh and Alon, 2014). Locally, the endothelium upregulates selectins and integrin ligands while systemically neutrophils are mobilized from the bone marrow (BM) (Strydom and Rankin, 2013). Mobilized neutrophils highly express molecules needed for homing, including P-selectin glycoprotein ligand-1, chemokine receptors and integrins. Neutrophils enter into rolling interactions with selectin expressing endothelium, allowing encounter with chemokines displayed on the endothelium that can then trigger firm integrin-mediated adhesion and crawling (Nourshargh and Alon, 2014). Multiple additional signals subsequently promote transendothelial migration and the precise requirements for this step continue to be determined (Filippi, 2019; Girbl et al., 2018).

Activated platelets can rapidly adhere to inflamed endothelium and display P-selectin and integrin ligands, providing additional support for neutrophil attachment (Deppermann and Kubes, 2018; Maas et al., 2018). Platelets also release granules containing numerous mediators, including chemokines and lipids that promote neutrophil adhesion and transmigration steps (Deppermann and Kubes, 2018; Maas et al., 2018; Rossaint et al.,

2016). Platelets contribute to neutrophil recruitment to inflamed peritoneum, lymph nodes (LNs), skin and other sites (Bogoslowski et al., 2018; Deppermann and Kubes, 2018; Gros et al., 2015; Kornerup et al., 2010; Maas et al., 2018; Zarbock et al., 2006). Another cell type that contributes to neutrophil recruitment is the perivascular mast cell. Mast cells can be activated by a range of inflammatory agents, and they promptly release multiple mediators that contribute to mobilizing selectins on endothelial cells, promoting vascular leakiness and chemoattracting neutrophils (Galli et al., 2020; Wernersson and Pejler, 2014). There is evidence for platelet-mast cell communication across the endothelium such that activation of one cell type can cause activation of the other (Karhausen et al., 2020; Schwartz, 1987).

The G-protein coupled receptor (GPCR) GPR35 is expressed by various myeloid cell types as well as by intestinal epithelium, peripheral sensory neurons, adipose and cardiovascular tissue (Quon et al., 2020). Ligand screening studies have identified multiple candidate ligands for GPR35, the most studied being kynurenic acid (KynA), as well as several synthetic agonists including Lodoximide (Deng et al., 2012; Foata et al., 2020; Taniguchi et al., 2006; Wang et al., 2006; Zhao et al., 2010). Lysophosphatidic acid (LPA) has also been suggested to be a GPR35 ligand with 2-acyl LPA being more active (Kaya et al., 2020; Oka et al., 2010). However, the low (micromolar) potency of the identified ligands has led to the view that GPR35 remains an orphan receptor (Quon et al., 2020). In some studies, GPR35 was reported to couple to Gα12/Gα13 and support Rho activation (Jenkins et al., 2011; Mackenzie et al., 2019; Park et al., 2018) and thus possible migration inhibition, while in other cases, it was found to couple to Gαi family members and promote chemotactic migration (Agudelo et al., 2018; Barth et al., 2009; Ohshiro et al., 2008; Taniguchi et al., 2006). An *in vitro* study reported that GPR35 agonism with KynA can promote arrest of monocytes and neutrophils on endothelium under flow conditions (Barth et al., 2009). However, whether GPR35 mediates neutrophil chemoattraction or recruitment to sites of inflammation *in vivo* is not known.

Here we set out to define the significance of GPR35 expression in neutrophils in the context of their trafficking to sites of inflammation, and to define ligand requirements for GPR35 function. We found that GPR35 was rapidly upregulated on mobilized neutrophils and that it supported their chemotactic migration. *In vivo*, GPR35 contributed to the efficiency of neutrophil recruitment to three sites of inflammation and augmented clearance of bacteria from the peritoneum. Using a bioassay, serum and activated platelet supernatant were found to engage GPR35 and we identified the platelet-derived metabolite 5-HIAA as a nanomolar GPR35 ligand. Platelets were important for GPR35-mediated neutrophil recruitment and imaging experiments showed GPR35 augmented neutrophil transmigration in regions of platelet accumulation. Mast cells, another source of 5-HIAA, contributed to GPR35-dependent neutrophil recruitment. Treatment with serotonin uptake inhibitor fluoxetine to prevent platelet loading with serotonin, or with a monoamine oxidase (MAO) inhibitor to block conversion of serotonin to 5-HIAA, overcame GPR35-mediated neutrophil recruitment. Genetic deficiency in the serotonin transporter (SERT) in platelets or of the serotonin biosynthetic enzyme tryptophan hydroxylase-1 (Tph1) in hematopoietic cells also caused loss of GPR35-dependent recruitment. The findings establish GPR35–5-HIAA as a chemoattractant receptor–ligand system that cooperates with other inflammation-induced factors in mediating neutrophil recruitment to sites of inflammation. In addition, given

GPR35 expression across diverse cell types, these data shed light on 5-HIAA as an inflammatory mediator for immune and non-immune cell populations.

RESULTS

GPR35 expression and pro-migratory activity in neutrophils

Acute peritonitis represents a serious medical condition and rapid neutrophil recruitment is essential for protection against invading peritoneal pathogens (Buscher et al., 2016). In the thioglycolate (TG) model of peritonitis there is strong neutrophil recruitment to the peritoneum that begins in the first hours after TG injection and persists for at least 24 hr (Ajuebor et al., 1999). In a time-course experiment, *Gpr35* was more than 10-fold upregulated in peritoneal neutrophils at 2 hr and expression had begun to decline by 18 hr (Figure 1a). *Gpr35* expression in blood neutrophils was higher than in immature BM neutrophils and was upregulated after 2 hr of mobilization (Figure 1a). Staining for total GPR35 protein with an antibody against the C-terminal cytoplasmic domain confirmed that protein expression was strongly upregulated within 2 hr (Figure 1b). Subcutaneous *Listeria monocytogenes* inoculation also led to upregulation of *Gpr35* in neutrophils recruited to the draining LNs, while skin pricking with a *Listeria*-contaminated needle led to GPR35 upregulation in neutrophils recruited to skin (Figure S1a, b). Analysis of a scRNAseq dataset (Xie et al., 2020) showed *Gpr35* expression was elevated in neutrophils recruited to the peritoneum in response to *E. coli* while being minimally expressed in BM neutrophils (Figure S1c, d). In gene expression data from human neutrophils exposed to the gram-negative bacterium *Francisella tularensis* (Schwartz et al., 2013), *GPR35* was strongly upregulated at 6 hr (Figure S1e).

In experiments with GPR35 transfected WEHI231 B lymphoma cells, GPR35-dependent chemotactic responses were detected to micromolar amounts of Lodoxamide and KynA, but not to 1-acyl or 2-acyl LPA (Figure 1c, d and Figure S1f, g). Migration could be inhibited by pertussis toxin (PTX) treatment, in accord with chemotactic migration depending on Gαi-coupling (Figure S1h). Additionally, Lodoxamide and high micromolar amounts of KynA – but not LPA – were effective at promoting internalization of GPR35 (Figure S1i-k). Mobilized neutrophils were also found to transmigrate across an endothelial monolayer to millimolar amounts of KynA in a GPR35-dependent manner (Figure 1e, f). In accord with previous work (Barth et al., 2009), KynA could promote adhesion of $GPR35^+$ cells to an endothelial monolayer in an integrin-dependent manner (Figure 1g and Figure S1l). These findings demonstrated that GPR35 could function as a pro-migratory and pro-adhesive receptor in mobilized neutrophils, though as with findings in other contexts (Barth et al., 2009; Quon et al., 2020) the high amounts of KynA required for these actions made it unlikely that it was a physiological ligand.

GPR35 promotes neutrophil recruitment to sites of inflammation

The ability of GPR35 to support *in vitro* migration of mobilized neutrophils suggested it may influence their recruitment to sites of inflammation. Using a mixed transfer approach in mice, GPR35-deficiency led to a 2-fold reduction in neutrophil recruitment to the inflamed peritoneum at 18 hr after TG injection (Figure 2a, b and Figure S2a, b). Time course studies

showed that GPR35 KO cell homing was already reduced at 2 hr after TG treatment (Figure S2c). Similar findings were obtained for peritoneal homing of endogenous neutrophils in TG immunized GPR35 WT:KO mixed BM chimeras that contain approximately equal frequencies of WT and GPR35-deficient neutrophils (Figure S2d) and also in full GPR35 KO mice (Figure S2e, f). In peritoneally inflamed GPR35 KO mice there was an increased frequency of neutrophils in the blood, likely a consequence of the reduced peritoneal recruitment (Figure S2g, h). Total cell numbers in the inflamed peritoneum were not affected by GPR35-deficiency indicating selectivity in the neutrophil recruitment defect (Figure S2i). GPR35-deficient neutrophil recruitment to the peritoneum was also reduced following TNF-induced inflammation (Figure 2c). Deficiency in IDO1, an enzyme in the KynA biosynthetic pathway (Cheong and Sun, 2018), did not alter the GPR35 contribution to neutrophil recruitment (Figure S2j). In a second model, we observed a GPR35 KO neutrophil recruitment defect into LNs that were inflamed following s.c. injection with *Listeria* (Figure 2d and Figure S2k-n). A similar defect was observed in recruitment to the site of *Listeria* injection in the skin (Figure 2e and Figure S2o). BM neutrophil frequency and the surface phenotype of BM and peritoneal neutrophils were unchanged in GPR35-deficient compared to WT (Figure S3a-c) and migration of BM neutrophils in response to other chemoattractants was unaltered (Figure S3d).

Listeria is a cause of peritonitis in humans (Eisa et al., 2018; Poulsen et al., 2018; Tablang, 2008). Following intraperitoneal infection with *Listeria* the recruited neutrophils were GPR35^{hi} (Fig. 2f) and there was 2-fold less neutrophil recruitment in GPR35-deficient mice (Fig. 2g). In accord with the defect in neutrophil recruitment, GPR35-deficient mice were less efficient at clearing *Listeria* from the peritoneum (Figure 2h). *E. coli* is another cause of human peritonitis (Facciorusso et al., 2019). GPR35 KO neutrophils were less efficiently recruited to the *E.coli* infected peritoneum (Fig. 2i) and GPR35-deficient mice were less able to clear the bacteria (Figure 2j, k). Ablation of neutrophils prior to the bacterial infections caused a loss of the GPR35 KO phenotype, consistent with GPR35 being required in neutrophils for bacterial clearance (Figure 2h, k). Using mixed BM chimeric mice in which the only lineage fully deficient in GPR35 was neutrophils, we again observed a defect in clearance of bacteria from the peritoneum (Figure 2l).

In the peritoneal inflammation experiments, all the neutrophils measured in the peritoneal lavage fluid are extravascular. Many neutrophils enter the peritoneum via the omentum, a sheet-like tissue composed of mesothelial cells and containing adipocytes, endothelial cells and aggregates of macrophages and lymphocytes in so called ‘milky spots’ (Buscher et al., 2016; Jackson-Jones et al., 2020). Flow cytometric analysis of intravascularly labeled cells showed that a significantly greater fraction of the GPR35-deficient neutrophils in the omentum were blood exposed 2 hr after transfer (Figure 3a, b). Taken together, the findings suggested the reduced accumulation of extravascular neutrophils in the peritoneum reflected reduced migration from vessels into omental tissue and not reduced attachment to the endothelium.

Intravital 2-photon microscopy was employed to gain dynamic information regarding the post-attachment recruitment step that was affected by GPR35-deficiency. To permit visualization of WT and GPR35-deficient neutrophils in the same animals, BM from Mrp8-

Cre x mTmG mice in which all neutrophils express GFP was mixed with BM from GPR35-deficient mice and used to reconstitute irradiated WT recipients. To permit visualization of all neutrophils, mice were pretreated with phycoerythrin (PE)-conjugated Ly6G antibody. Imaging of the omentum in these BM chimeras showed GPR35-deficient neutrophils were less efficient at moving from the vessel lumen into the parenchyma (Figure 3c-f and Movies S1, S2). Similar observations were made with transferred fluorescently labeled neutrophils (Movie S3) though the low frequencies of transferred cells in each imaging volume made this approach less quantitative. Figure 3g shows a zoomed-in view of a transmigration event. GPR35 KO neutrophil track speed within vessels was increased (Figure S4a), while no differences were observed in total cell track speed that included many cells in the parenchyma (Figure S4b). Microscopy on the skin of WT:GPR35 KO mixed BM chimeras showed a similar dependence on GPR35 for neutrophil movement from blood vessel into tissue (Figure S4c-f and Movie S4) and the cells showed a trend for increased speed (Figure S4g); in this tissue, total GPR35-deficient cells also had a slightly increased track speed (Figure S4h). These data suggest that GPR35 contributes along with other chemoattractant factors to promoting transendothelial migration of activated neutrophils and that this activity involves a reduction in speed perhaps due to GPR35-promoting increased adhesion of crawling cells.

5-HIAA is an endogenous GPR35 ligand

Using an *in vitro* migration-based bioassay we screened tissue extracts for GPR35 ligand activity and found activity in serum (Figure 4a). Serum is made up of plasma and the contents of activated platelets. Serum had stronger GPR35 ligand activity than plasma, consistent with platelets functioning as a source of ligand (Figure 4a). Indeed, activated platelet supernatant promoted attraction of $GPR35^+$ cells (Figure 4b, c). Platelet supernatant was also able to cause GPR35 internalization (Figure S5a). Platelets have not been identified as a source of KynA and have minimal expression of KynA synthetic enzymes (Manne et al., 2020; Wirthgen et al., 2018), but they are an important reservoir of gut-derived serotonin (5-Hydroxytryptamine), another tryptophan metabolite (Berger et al., 2009). Serotonin was inactive in recruiting $GPR35^+$ cells (Figure S5b) in accord with earlier data (Wang et al., 2006). Platelets express monoamine oxidase-B (MAO-B) and they metabolize serotonin into 5-HIAA, and their dense granules contain 5-HIAA as well as serotonin (Berger et al., 2009; Pletscher, 1968; Shad and Saeed, 2007). Strikingly, 5-HIAA was a potent chemoattractant of mouse and human $GPR35^+$ cells (Figure 4d, e and Figure S5c) and it could promote $GPR35^+$ cell adhesion to endothelial monolayers (Figure S5d). 5-HIAA was also effective in promoting activated neutrophil migration (Figure 4f) and their transmigration across an endothelial monolayer in a GPR35-dependent manner (Figure S5e). Mixing CXCL1 and 5-HIAA had an additive effect in promoting activated neutrophil adhesion and transmigration (Figure S5f, g). Confirming that 5-HIAA was acting as a GPR35-ligand, it caused internalization of the murine and human receptor from the cell surface in a dose dependent manner, while not internalizing a control GPCR (Figure 4g-i and Figure S5h).

GPR35 function in neutrophil recruitment involves platelets

Since platelet-derived 5-HIAA could promote migration of GPR35$^+$ cells *in vitro*, we explored the contribution of platelets to GPR35-mediated neutrophil recruitment *in vivo*. By real time imaging of PF4-Cre$^+$ mTmG reporter mice that harbor GFP$^+$ platelets, a dense accumulation of platelets was observed on the inflamed endothelium in the omentum (Figure 5a) as well as in LNs and skin (Figure S6a). Neutrophils were observed attached to platelet-coated endothelial surfaces and often crossed the endothelium in these regions (Figure 5a and Movies S5 and S6). GPR35-deficient neutrophils showed reduced association with platelets and most notably, reduced transmigration in platelet rich regions (Figure 5a, Figure S7a and Movies S5 and S6). Quantitation showed that GPR35-deficient cells had reduced platelet contact and reduced total time in contact and a greater distance of transmigrating cells from platelets (Figure 5b, c and Figure S6c, d). Neutrophil interaction with platelets can lead to neutrophils acquiring platelet membrane markers (Page and Pitchford, 2013). Flow cytometric analysis showed reduced acquisition of the platelet marker CD41 (Itga2b/GPIIb) by GPR35-deficient neutrophils in peritoneally inflamed mice, consistent with reduced intravascular neutrophil-platelet contact (Figure 5d and Figure S6e).

Neutrophil transfers into platelet-deficient mice showed that GPR35 was less able to augment neutrophil recruitment to inflamed skin since wild-type and GPR35 KO cells were recruited more similarly (Figure 5e). Moreover, WT but not KO neutrophils showed higher labeling by intravascular antibody in skin-inflamed platelet-deficient mice indicating less efficient movement from blood vessels into the tissue parenchyma (Figure 5f). Enumeration of the recruited transferred cells confirmed the platelet dependence of GPR35 function and showed that platelet deficiency had a further effect on neutrophil recruitment (Figure S6f), consistent with multiple platelet-derived factors being involved in recruitment. A similar platelet-dependence of GPR35 function was observed in *Listeria*-inflamed LNs (Figure 5g). Homing to peritoneum could not be readily studied in platelet-deficient mice due to the strong inflammation frequently causing blood leakage into the peritoneum in the absence of platelets. Taken together, these data strongly implicate platelets, likely acting as a source of 5-HIAA, in GPR35-mediated neutrophil recruitment.

Mast cells contribute to GPR35-mediated recruitment of neutrophils

Platelets do not synthesize serotonin but acquire it from intestinal epithelial cells (Berger et al., 2009). The one peripheral cell type beyond intestinal epithelium that highly expresses Tph1 and synthesizes serotonin is the mast cell (Herr et al., 2017; Nowak et al., 2012; Yabut et al., 2020). Mast cells also express MAO (Immgen.org) and a few studies have suggested they can be a source of 5-HIAA (Freitag et al., 1995; Gershon et al., 1975; Lehtosalo et al., 1984; Sjoerdsma et al., 1957). We found that activation of peritoneal mast cells with LPS led to generation of extracellular 5-HIAA and the mast cell supernatant was active in attracting GPR35$^+$ cells (Figure 6a, b). The P815 mastocytoma cell line constitutively released 5-HIAA (Figure 6c). Treatment with anti-5-HIAA blocked GPR35-dependent cell migration to mast cell supernatants and to serum (Figure 6d, e). We then observed that mast cell-deficient mice supported reduced GPR35-dependent recruitment of neutrophils to *Listeria*-inflamed skin (Figure 6f). Intravascular labeling showed that the GPR35-dependent exit of cells from the skin vascular compartment required mast cells (Figure 6g). *Listeria*

inoculation in the skin caused rapid mast cell activation, measured by CD63 upregulation (Figure 6h). To examine the sufficiency of mast cell-derived 5-HIAA to promote neutrophil recruitment, we performed experiments in platelet-depleted mice. *Listeria* induced less mast cell activation in platelet-depleted mice (Figure 6h) in accord with evidence that platelets trigger activation of perivascular mast cells (Karhausen et al., 2020). Treatment of *Listeria* inoculated platelet-depleted mice with the mast cell-triggering compound 48/80 (Freitag et al., 1995) was able to restore mast cell activation (Figure 6h) and this treatment increased the GPR35-dependence of neutrophil recruitment (Figure 6i). Additionally, injection of 5-HIAA into the skin of mast cell-deficient mice at the same time as *Listeria* inoculation promoted GPR35-dependent neutrophil recruitment, determined both by the efficiency of recruitment of transferred cells (Figure 6j) and by enumerating recruitment of endogenous neutrophils (Figure 6k). These data are consistent with the possibility of mast cell-derived 5-HIAA cooperating with platelet-derived 5-HIAA during neutrophil recruitment.

5-HIAA is required for GPR35-mediated neutrophil recruitment

Fluoxetine (Prozac™) is a serotonin uptake inhibitor and chronic fluoxetine treatment is well established to prevent serotonin accumulation (and 5-HIAA generation) selectively in platelets due to their lacking Tph1 and acquiring intestinal serotonin from circulation (Berger et al., 2009). Three-week treatment of mice with fluoxetine reduced recruitment of transferred WT neutrophils to inflamed skin but did not cause further reduction in recruitment of GPR35 KO cells when assessed as a percent of total cells recruited (Figure 7a, b). This was also seen when the data were plotted as a recruitment index (Figure 7c). Treatment with phenelzine to inhibit MAO and block serotonin conversion to 5-HIAA in both platelets and mast cells (Bortolato et al., 2008), had a similar effect in reducing the percent of WT but not causing significant further reduction in the percent of GPR35-deficient neutrophil recruitment (Figure 7a-c). Plotting the numbers of WT neutrophils recruited showed strong reductions after both fluoxetine and phenelzine treatment (Figure S7a). Significantly less GPR35 KO cells were recruited under control treatment conditions but there was a trend towards a further reduction after fluoxetine treatment and a significant further reduction after phenelzine treatment (Figure S7a). GPR35-independent effects of drug treatment are consistent with contributions of platelet-derived serotonin to neutrophil recruitment (Berger et al., 2009; Duerschmied et al., 2013; Kubes and Gaboury, 1996). Intravascular labelling in inflamed mice showed that the intravascular accumulation bias of GPR35-deficient skin neutrophils observed in control recipients was lost in phenelzine treated recipients (Figure 7d, e). Fluoxetine and phenelzine treatment also reduced the skin homing efficiency of endogenous neutrophils and there was increased intravascular labeling of neutrophils in the inflamed skin (Figure 7f, g). Importantly, supernatant from activated platelets purified from fluoxetine or phenelzine treated mice was less effective in promoting GPR35dependent chemotaxis (Figure 7h) and contained significantly reduced amounts of 5-HIAA (Figure 7i).

As an MAO inhibitor, phenelzine would be expected to reduce 5-HIAA production by both platelets and mast cells. We therefore treated platelet-deficient mice with phenelzine in an attempt to measure the impact of blocking mast cell generation of 5-HIAA. Although *Listeria* was less effective in promoting mast cell activation and GPR35-dependent

neutrophil recruitment in the absence of platelets, some mast cell activation did occur (Figure 6f) and there was a trend for a GPR35 contribution to recruitment in the absence of platelets (Figures 5e and 6i). In accord with the detection of some platelet independent GPR35 recruitment activity, phenelzine treatment of platelet-deficient mice led to a reduction in *Listeria*-induced neutrophil recruitment to the skin (Figure 7j).

In another approach, mice were treated with a large intravenous dose of 5-HIAA to disrupt endogenous 5-HIAA gradients. Two hours after treatment the plasma 5-HIAA concentration was in the near micromolar range (Figure S7b), well above the low nanomolar concentration found in normal mouse and human plasma (Figure S7b) (Callebert et al., 2006; Pietraszek et al., 1991; Sano et al., 1993; Tanaka et al., 2021; Tohmola et al., 2014). This treatment caused reduced recruitment of transferred WT but not GPR35-deficient neutrophils to the inflamed skin and peritoneum (Figure S7c, d). The treatment also reduced homing of endogenous WT neutrophils to the inflamed peritoneum (Figure S7e) and skin (Figure S7f). By contrast, treatment with an equivalent dose of KynA was without effect (Figure S7g). The 5-HIAA treatment did not alter the frequency of neutrophils, including marginated cells, in lungs, spleen or BM (Figure S7h, i).

We next examined SERT KO mice that lack 5-HIAA in platelets (Bengel et al., 1998; Berger et al., 2009). In accord with the fluoxetine treatment results, there was reduced GPR35-dependent homing of transferred neutrophils to the inflamed skin of SERT KO mice (Figure 7k and Figure S8a) and reduced recruitment of endogenous neutrophils (Figure S8b). To confirm this reflected a role for SERT in platelets we examined mixed BM chimeras where full SERT deficiency was restricted to platelets. As in SERT KO mice, there was reduced GPR35-dependent neutrophil recruitment to the inflamed ear skin (Figure S8c-e).

To genetically disable 5-HIAA production in mast cells we reconstituted lethally irradiated WT mice with BM from Tph1 KO mice (Cote et al., 2003). Such chimeric mice retain Tph1 expression in gut epithelium, the source of platelet 5-HIAA (Berger et al., 2009). Mast cells from the Tph1 KO BM chimeras were confirmed to have significantly reduced ability to produce 5-HIAA (Figure S8f). Tph1 KO BM chimeras showed reduced GPR35-dependent recruitment of transferred neutrophils to *Listeria* inoculated ear skin (Figure 7l and Figure S8g) and reduced recruitment of endogenous neutrophils (Figure S8h). Taken together, these data indicate that 5-HIAA is an *in vivo* ligand of GPR35, and they provide evidence that both platelets and mast cells contribute to 5-HIAA production at sites of inflammation.

DISCUSSION

This study reveals that the major serotonin metabolite, 5-HIAA, acts as a physiological ligand for GPR35 and thereby promotes neutrophil recruitment to sites of inflammation and bacterial clearance. Our data suggest that platelet- and mast cell-derived 5-HIAA cooperate non-redundantly in neutrophil recruitment, working with other mediators produced by these cells. In the simplest model, we propose that platelet-derived 5-HIAA promotes adhesion of crawling neutrophils in association with platelet clusters and that mast cell-derived 5-HIAA provides directional signals during transmigration. The ability of platelets and mast cells to cross-activate each other may amplify these events (Karhausen et al., 2020; Schwartz, 1987).

Our studies do not fully exclude roles for other cell types as sources of neutrophil-recruiting 5-HIAA. GPR35 and 5-HIAA are likely to contribute to the recruitment of additional $GPR35^+$ blood cells, such as monocytes, to sites of inflammation and they may also guide myeloid cell migration within tissues (Barth et al., 2009; Kaya et al., 2020; Pagano et al., 2021; Quon et al., 2020; Slaba et al., 2015).

Serotonin was discovered over 70 years ago and it is known to have wide ranging influences on animal physiology, but 5-HIAA has been considered to merely be its waste metabolite (Berger et al., 2009; Bortolato et al., 2010). Our findings add to nascent evidence that 5-HIAA is itself an intercellular signaling molecule with one study suggesting it acts as a ligand for the aryl hydrocarbon receptor (Rosser et al., 2020) and work in *C. elegans* suggesting it modulates Ras/MAPK signaling (Schmid et al., 2015). Serotonin acts on the endothelium to promote vascular leakiness and leukocyte rolling interactions, with the latter involving mobilization of endothelial cell adhesion molecules (Askenase et al., 1980; Berger et al., 2009; Duerschmied et al., 2013; Kubes and Gaboury, 1996). We suggest that serotonin and 5-HIAA may often cooperate during the neutrophil recruitment process. Our findings prompt the need to consider how widely used serotonin (and thus 5-HIAA) modulating drugs (Berger et al., 2009; Bortolato et al., 2008) or neuroendocrine tumors that lead to markedly elevated plasma 5-HIAA (Lindstrom et al., 2018) influence GPR35-mediated processes. Depending on the inflammatory condition, reduced neutrophil recruitment in mice treated chronically with fluoxetine may reflect reduced rolling-mediated attachment to the less activated endothelium (Duerschmied et al., 2013) as well as reduced GPR35 function. Although serotonin has been suggested to act directly on neutrophils (Herr et al., 2017), there is a lack of genetic evidence that neutrophils functionally express serotonin receptors. We suggest that the putative direct actions of serotonin modulators on neutrophils instead involve reductions in 5-HIAA and thus GPR35 function. The doses of fluoxetine and other Selective Serotonin Reuptake Inhibitors (SSRIs) used to treat psychiatric conditions in patients may not be sufficient to fully deplete platelets of serotonin and 5-HIAA. However, evidence exists for increased bacterial infections in some SSRI treated patients and for the occasional development of skin lesions, conditions consistent with reduced neutrophil function (Herstowska et al., 2014; Jarchum et al., 2012; Rogers et al., 2013),

Our finding of an intraluminal enrichment of GPR35-deficient versus WT neutrophils at sites of inflammation suggests that GPR35-deficiency does not impede attachment to the endothelium. However, our findings do not exclude the possibility, suggested based on *in vitro* data (Barth et al., 2009), that GPR35 contributes to the neutrophil rolling-to-sticking transition under some conditions. Platelets are a source of multiple neutrophil recruitment factors, including platelet activating factor, adhesion molecules and chemokines (Slaba and Kubes, 2017) and 5-HIAA must act in concert with these factors to promote adhesion of crawling neutrophils in association with platelets and their subsequent transmigration across endothelium. Multiple reports have established that platelets augment neutrophil transendothelial migration into tissue, and while their contribution of P-selectin and integrin ligands are well established (Slaba and Kubes, 2017), how the chemoattractive mediators augment the transendothelial migration step remains less understood. As with other platelet-derived chemoattractants, it is unclear whether platelet 5-HIAA is only acting intralumenally, or whether the continual loss of luminal molecules in blood flow allows a

transendothelial gradient to be established. In this regard it is notable that platelets were the principal source of serotonin in inflamed tissue of mast cell-deficient mice (Geba et al., 1996). Like platelets, mast cells also produce multiple neutrophil chemoattractants (Galli et al., 2020; Wernersson and Pejler, 2014) raising interesting questions about how individual factors have non-redundant roles during the recruitment process. Early cell depletion and drug treatment studies implicated platelet- and mast cell-derived serotonin in cell recruitment events associated with delayed type hypersensitivity (DTH) (Askenase et al., 1980; Askenase et al., 1983; Geba et al., 1996). It seems likely that 5-HIAA will also be involved in the DTH response. It will be important to determine the mechanism of 5-HIAA release from mast cells and whether it can be triggered differentially from histamine release as has been suggested for serotonin (Meixiong et al., 2019; Theoharides et al., 1982). Moreover, whether mast cell Tph1 and MAO continue to act following mast cell activation and thereby allow ongoing 5-HIAA production needs investigation.

While the production of serotonin by murine mast cells is well established, production by human mast cells has been questioned (Sjoerdsma et al., 1957). However, subsequent work showed serotonin in the supernatant of human mast cells in amounts within 5-fold of those produced by mouse mast cells (Enerbäck, 1963; Kushnir-Sukhov et al., 2007; Wernersson and Pejler, 2014). A proteomic study revealed that MAO-B is one of the proteins most enriched in human and mouse mast cells compared to non-mast cells (Plum et al., 2020). Moreover, many patients with mastocytosis had elevated serum serotonin and patients with urticaria pigmentosa (a condition of elevated skin mast cell activity) had elevated circulating 5-HIAA (Kushnir-Sukhov et al., 2007; Morishima, 1970). We therefore contend that like in the mouse, human mast cells contribute to 5-HIAA production and GPR35-mediated cell recruitment at sites of inflammation, but further study of this topic is needed.

GPR35 has been shown to influence intestinal inflammation and colon cancer development as well as cardiac, vascular and adipose tissue function (Agudelo et al., 2018; Boleij et al., 2021; Divorty et al., 2018; Farooq et al., 2018; Kaya et al., 2020; Schneditz et al., 2019; Tsukahara et al., 2017). Some of these effects may involve actions in myeloid cells while others may occur through actions in the epithelium or other GPR35-expressing cell types. By identifying 5-HIAA as an *in vivo* ligand for GPR35, our findings will enable advances in understanding actions of GPR35 in physiology and disease. Moreover, this ligand-receptor axis might be targeted by next generation drugs such as MAO-inhibitors with reduced blood brain barrier permeability (Gealageas et al., 2018) to modulate $GPR35^{+}$ cell responses in the context of infections, autoinflammatory diseases, sensory neuron responses and cancer.

Limitations of study

While we provide extensive functional evidence that 5-HIAA is a GPR35 ligand, we have not performed binding studies. It will be of interest in the future to determine the 5-HIAA binding constants using purified GPR35 protein. We also do not exclude the possibility that other metabolites of serotonin or related amines may function as GPR35 ligands under some conditions. Chronic treatment with fluoxetine and genetic deficiency in SERT reduce platelet serotonin content while phenelzine treatment may increase it and both conditions can lead to increases in plasma serotonin. By comparing WT and GPR35-

deficient neutrophil migration in the same animals, indirect (systemic) effects of the drug treatments or SERT deficiency are controlled for but a co-dependence of the observed effects on altered serotonin levels as well as 5-HIAA levels cannot be excluded. This is also the case for possible effects of reduced hematopoietic serotonin production in Tph1-deficient BM chimeras.

STAR*METHODS

Resource Availability

Lead Contact—Further information and requests for reagents may be directed to and will be fulfilled by the lead contact Jason Cyster (jason.cyster@ucsf.edu)

Materials Availability—Further information and requests for reagents will be fulfilled by Dr. Jason Cyster (jason.cyster@ucsf.edu). A list of critical reagents (key resources) is included in the Key resources table. Some material may require requests to collaborators and/or agreements with various entities. Material that can be shared will be released via a Material Transfer Agreement.

Data and Code Availability—All data reported in this paper will be shared by the lead contact upon request.

This paper does not report original code.

Any additional information required to reanalyze the data reported in this paper is available from the lead contact upon request.

Experimental Model and Subject Details

Mice—C57BL/6J and BoyJ (CD45.1) mice were bred in an internal colony and 7–12-week-old mice of both sexes were used. *Gpr35*$^{-/-}$ mice were obtained from EMMA (EM09677; Gpr35tm1b(EUCOMM)Hmgu) and maintained on a B6 background. C57BL/6-Gt(ROSA)26Sortm1(HBEGF)Awai/J (iDTR mice) were purchased from Jackson Laboratories. Platelet-deficient mice (*c-mpl*$^{-/-}$), Pf4-Cre x mTmG (Gt(ROSA)26Sor$^{tm4(ACTB-tdTomato,-EGFP)Luo}$/J) platelet reporter mice (Lefrancais et al., 2017) and Mrp8-Cre x mTmG neutrophil reporter mice (Lefrancais et al., 2018) were all on a B6 background. Mast cell-deficient Kit/v x Kit/W mice and SERT-deficient mice (Bengel et al., 1998) were obtained from Jackson Laboratories and maintained on a B6 background. Tph1 KO (Cote et al., 2003) BM was provided by Huaquing Wang and Waliul Khan (McMaster Univ.). Littermate controls (WT and HET) were used for experiments, mice were allocated to control and experimental groups randomly, sample sizes were chosen based on previous experience to obtain reproducible results and the investigators were not blinded.

Method Details

Treatments and bone marrow chimeras—In co-transfer experiments, purified WT and KO neutrophils were stained for 30 min at 37°C with Cell trace Violet (#C34557, Fisher), CMTMR (#C2927, ThermoFisher), CFSE (#C34554, ThermoFisher), or Deep

red (#C34565, Life Tech) as indicated and mixed 50:50 before injection (0.5–3 × 10^7 neutrophil / mouse in 200ul saline), 30 min before i.p. TG. To induce peritonitis, mice were injected i.p. with either 1ml of thioglycolate 4% (Sigma), 500ng TNF in 500μl saline (Biolegend) or 1×10^5 CFUs *Listeria* or 1×10^4 CFUs *E.coli* in 500μl saline. To stimulate neutrophil recruitment to draining LNs, mice were s.c. injected with 5 × 10^6 CFUs in 40μl saline. To boost neutrophil homing to the skin, anesthetized mice were ear-pricked (20 time/ear) with *Listeria*-contaminated needles (27G). To deplete platelet 5-HIAA, mice were treated for 3 weeks with Fluoxetine (160mg/L dissolved in drinking water, #1279804, Millipore Sigma) before skin-pricking, similarly to what has been previously reported (Cloutier et al., 2012; Musgrave et al., 2011). To deplete total generation of 5-HIAA, mice were treated with two i.p. doses of Phenelzine (30mg/kg, #P6777, Millipore Sigma) at −18hr and −1hr before skin-pricking. To disrupt 5-HIAA or Kynurenic acid *in vivo* gradients, 200μl saline containing 100μM 5-HIAA or Kynurenic acid (Sigma) were injected i.v. 10 min before i.p. TNF treatment. Mice have a blood volume of at most 2ml and the injection is therefore expected to achieve a >10μM blood concentration. To produce mixed chimeras, CD45.1 congenic Boy/J mice were lethally irradiated with 1300 rad in split doses and reconstituted with 5 × 10^6 BM cells (~50:50) as indicated. Mice were analyzed 6–7 weeks later. Animals were housed in a pathogen-free environment in the Laboratory Animal Resource Center at the University of California, San Francisco, and all experiments conformed to ethical principles and guidelines that were approved by the Institutional Animal Care and Use Committee. To generate mice with full GPR35-deficiency restricted to neutrophils, MRP8-Cre x iDTR BM was mixed 1:1 with GPR35 WT or KO BM and used to reconstitute WT mice. After 6 weeks reconstitution the chimeras were treated with 400ng diptheria toxin i.v. (DT) at d-1 and with 80ng DT i.v. 2hr before infection with *Listeria*. iDTR-expressing neutrophil depletion was confirmed by flow cytometry. To deplete platelets, mice were treated with 2ug/g of anti-CD42b depleting antibody (Emfret Analytics) 24 hr before the experiment. Platelet-deficient or platelet-depleted mice showed extensive peritoneal bleeding after i.p. TG or TNF injection, resulting in animals having to be euthanized within 12–18hrs after injection. Therefore, all data with platelet deficient or depleted mice were obtained using the skin model. To locally activate mast cells, 50μl of compound 48/80 (50μg/ml, Sigma) were injected s.c. 5 min before *Listeria* pricking. In indicated experiments, mast cell-deficient mice were injected s.c.with 2uM 5-HIAA (or DMSO) in 20ul in the ear skin immediately before *Listeria* skin-pricking.

Flow cytometry and cell sorting—Neutrophils were identified as either $Ly6G^+$ $Ly6C^+$ $CD11b^+$ or $Ly6G^+$ $CD11b^+$ cells as indicated, using the following antibodies: fluorescein isothiocyanate (FITC)-conjugated rat anti-mouse Ly6C (AL-21, #553104, BD); APC-Cy7-conjugated rat anti-mouse Ly6G (1A8, TONBO); BV785-conjugated rat anti-mouse CD11b (M1/70, #101243, BioLegend) and APC-conjugated rat anti-mouse CXCR2 (SA044G4, #149312, BioLegend). PE rat anti-mouse CD45.1 (A20, 110708, Biolegend) and FITC rat anti-mouse CD45.2 antibody (104,109805, BioLegend). FITC-conjugated rat anti-mouse CD11a (I21/7, #153105, BioLegend); Biotin-conjugated rat-anti mouse CD18 (C71/16, #557439, BD); FITC-conjugated rat anti mouse LFA-1 (REA880, #130–114-422, Miltenyi Biotec); APC-conjugated rat anti-mouse CXCR2 (SA044G4, #149311, BioLegend); PE-Cy7-conjugated rat anti-mouse CD62L (Mel-14, #104418, BioLegend); BV421-conjugated

rat anti-mouse PSGL1 (2PH1, #562807, BD). To analyze mast cells, PE-conjugated rat anti-mouse CD117 (2B8, #553355, Fisher) and FITC-conjugated rat anti-mouse CD63 (NVG-2, #143920, BioLegend) were used.

To identify intravascular cells, 2 μg / 200μl saline of PE- conjugated anti-mouse CD45.2 (104, #109808, Biolegend) were injected 2 min before sacrifice as indicated. For flow cytometry staining, cells were placed in a 96-well round bottom plate and washed with staining buffer (PBS containing 2% NBCS and 0.5 mM EDTA), and 40 μl of antibody cocktail was added to each sample for 20 min on ice. After incubation, cells were washed twice with staining buffer. For staining of the N-terminal OX56 tag, a 1:200 dilution of a biotinylated OX56 antibody (Bio X Cell) was placed on the cells for 25 min on ice, after which the cells were washed and a 1:200 dilution of streptavidin–PE (#405203, BioLegend) was incubated with the cells for 20 min. To identify Thy1.1 reporter expression, AF647-conjugated anti-mouse/rat CD90.1 (#202508) was used. Rabbit polyclonal anti-GPR35 was produced by Biomatik (using as immunogen the C-terminus peptide: MAREFQEASKPAT SSNTPHKSQDSQILSLT) and affinity-purified. To reduce staining background, anti-GPR35 polyclonal antibody was pre-absorbed against GPR35 KO splenocytes overnight at 4°C. Cells were surface-stained, fixed and permeabilized (eBioscience™, #00552100) before intracellular staining. AF647-Goat anti-Rabbit IgG (H+L) Highly Cross-Adsorbed Ab (A21245, Fisher Scientific) was used as secondary antibody. To quantify neutrophil-platelet interaction, 100 μl of blood were obtained by retro-orbital bleeding (heparinized capillaries) and drawn into tubes containing 1ml of Lyse/Fix Buffer 5X (Ox-7, #558049, BioLegend) and incubated for 15 min. Cells were than wash and resuspended in staining buffer. FITC- conjugated anti-mouse CD41 (MWReg30, # 133903, BioLegend) was used to stain neutrophils that had acquired membrane-bound platelet. Data were acquired using a BD LSR II flow cytometer or a Cytek Aurora. A BD FACSAria II was used to sort murine $Ly6G^+$ $CD11b^+$ $CXCR2^+$ neutrophils (purity >96%). Flow cytometry data were analyzed using Flowjo (v.10.6.2).

Generation of GPR35-expressing WEHI-231 cells—Murine and human GPR35 were cloned into the murine stem cell virus (MSCV)-GFP retroviral vector (mGPR35-GFP or hGPR35-Thy1.1). The retroviruses encoding mGPR35-GFP/hGPR35-Thy1.1 were produced using the Platinum-E packaging cell line, as previously described (Lu et al., 2019). Briefly, 5×10^5 WEHI-231 cells were placed in a 6-well plate along with the retroviral supernatant and the cells were centrifuged at 1,340g (2,400 r.p.m.) for 2 h at room temperature. This spinfection was repeated with fresh retrovirus for a second time 24 h later. Then, 48 h after the second spinfection, the highest 3% of GFP/Thy1.1-expressing cells were sorted using a BD FACSAria II. These cells were combined with GFP/Thy1.1-negative cells in a ~1:1 ratio to run transwell migration assays.

Cell lines and treatments—HEK293T and bEND3 cells were grown in 10-cm tissue culture dishes in DMEM containing 10% FBS, 10 mM HEPES, 2 mM glutamine and 50 IU penicillin/streptomycin. WEHI-231 were grown in upright T25 flasks in RPMI containing 10% FBS, 10 mM HEPES, 2 mM glutamine, 55 μM 2-mercaptoethanol and 50 U penicillin/streptomycin. All cell lines were previously obtained from other laboratories

and further authentication was not performed. The cell lines were not tested for mycoplasma contamination. To test the activity of 2-acyl LPA, empty vector (EV) or Lipase member H (LIPH)-transfected HEK293T cells were grown out in 10-cm tissue culture dishes and allowed to reach confluence. The medium was then replaced with serum-free medium (RPMI containing 0.5% fatty acid-free BSA and 10 mM HEPES) and tested in the bioassay. LIPH is also known as PA-PLA1 and it catalyzes removal of the sn-1 acyl chain from phosphatidic acid to generate 2-acyl LPA (Sonoda et al., 2002). For transfection of HEK293T cells, mouse *Liph* was cloned into an MSCV-Thy1.1 retroviral vector, similarly to what previously described (Lu et al., 2019). Briefly, HEK293T cells were seeded into 10-cm tissue culture dishes and grown until 75% confluent in antibiotic-free medium. Plasmids were aliquoted in Opti-MEM, then mixed with Lipofectamine 2000 (at 6 μl per 3 μg plasmid) and allowed to sit for 25 min at room temperature. The mixtures were gently added dropwise to the HEK293T cells. Then, 24 h after transfection, the medium was replaced with serum-free medium. To inhibit Gαi-signaling, GPR35-GFP and control WEHI-231 cells were pre-treated with 100ng/ml pertussis toxin (PTX, #181, List Biological Labs, Inc) for 30 min at 37°C before running the transwell migration assay. P815 mastocytoma cells were used as a mast cell-like cell line. To block 5-HIAA-driven migration, anti-5-HIAA polyclonal antibody (My-bio-Source) was used at 2ug/ml.

Chemicals and reagents—Lodoxamide (#SML2307), Kynurenic acid (#K3375), 18:1 LPA (#L7260), and 5-HIAA (#H8876) were purchased from Sigma. Serotonin (#14332) was purchased from Cayman Chemical.

Quantitative PCR—Total RNA from sorted BM, blood or peritoneal neutrophils was extracted using an RNeasy kit (Qiagen) and reverse-transcribed using M-MLV reverse transcriptase. qPCR was performed using Power SYBR Green with an Applied Biosystems StepOnePlus instrument. Data were analyzed with the comparative Ct ($2^{-\Delta\Delta Ct}$) method, using the housekeeping genes indicated in the figures.

Transwell migration assay—Control and GPR35-transduced WEHI-231 cells were taken from T25 flask cultures, washed twice in pre-warmed migration medium (RPMI containing 0.5% fatty acid-free BSA, 10 mM HEPES and 50 IU penicillin/streptomycin) and mixed 50:50. The cells were resuspended in migration medium at 2×10^6 cells / ml and resensitized for 10 min in a 37 °C water bath in migration medium (0.5% fatty-acid free BSA, 10mM Hepes RPMI). Transwell filters (6 mm insert, 5 μm pore size, Corning) were placed on top of each well, and 100 μl containing 2×10^5 cells of GPR35–GFP/ control WEHI-231 cell mix was added to the transwell insert. The cells were allowed to migrate for 3 hr, after which the cells in the bottom well were counted by flow cytometry. For neutrophil transwell migration assay, peritoneal cells from WT-CD45.1 / GPR35 KO mixed chimeras (2hr after TG) were diluted at 2×10^6 cells / ml in 0.5% fatty-acid free BSA, 0.5% FBS (migration plus) medium. Preliminary experiments established that inclusion of a low amount of FBS was necessary to maintain viability of the neutrophils during the assay. Representative experiments for each migration assay are plotted as a percentage of input migration. The baseline migration between experiments differs based on the growth state of the WEHI-231 cells.

Transendothelial migration assay and adhesion assay—To perform a neutrophil *in vitro* transmigration assay, bEND3 cells were trypsinized and resuspended at 4–5×10^5 / ml in complete medium. 24 well plate containing 0.6ml complete (10%FCS) medium per well were prepared, transwells (5um) were inserted in the plates and 100ul of bEND3 cell mix were gently pipetted on each transwell (5um, Corning). Cells were allowed to grow on transwells for 48 hrs. Confluent bEND3-containing transwells were stimulated for 1hr with TNF (100ng/ml) before the assay. After activation, excess medium was removed, transwells were washed twice and placed in new 24-well plates containing indicated dilutions if migration stimuli. Peritoneal cells (2hr after TG) were diluted at 2×10^6 / ml and 100ul of peritoneal cell mix in migration medium were gently pipetted on bEND3 transwells. Cells were allowed to migrate for 2hr at 37°C. Cells and migration stimuli were diluted in 0.5% migration plus medium. Data are plotted as % of input migration. To perform neutrophil or WEHI-231 adhesion assays, 3×10^4 bEND3 cells /well were seeded in flat 96 well plates for 24hr. Confluent bEND3-containing wells were stimulated for 1hr with TNF (100ng/ml) before the assay. After activation, bEND3 monolayers were washed and 50ul of chemokine solutions (2x) were added. Peritoneal cells (2hr after TG) or WEHI-231 were prepared at 2×10^6 / ml in migration medium and 50ul of cell mix was gently pipetted on bEND3 layer and incubated at 37°C for 45 minutes. Monolayers were then gently washed with migration medium (5x) and 100ul of 5mM EDTA solution was added to each well and incubated for 15 min on ice. Harvested cells were centrifuged, washed and resuspended in FACS buffer for flow cytometry analysis. To test integrin dependency, cells were inhibited with 20ug/ml of anti-aL and anti-a4 blocking antibody (BioXcell) for 15 min at 37°C before the assay. Cells and migration stimuli were diluted in 0.5% migration plus medium. Data are plotted as % of input migration.

Internalization assay—Murine and human GPR35 were cloned into an MSCV-GFP/Thy1.1 retroviral vector with an N-terminal OX56 epitope tag (Lu et al., 2019) to track surface expression levels of each receptor. Both receptors were transduced into WEHI-231 cells. Confluent cultures of each of the lines indicated above were washed twice in migration medium, resuspended at 5 × 10^6 cells ml^{-1} and resensitized at 37 °C for 10 min. For each line, 50 μl of cells was aliquoted into a 96-well plate. Stimuli were prepared in migration medium and 50-μl aliquots were placed into a 96-well round bottom plate that was placed in a 37 °C cell culture incubator for 45 min. The plate was then placed on ice, washed with ice-cold flow cytometry buffer and stained for OX56 by flow cytometry. OX56 surface levels on transduced cells were assessed by gating on the top 40% of OX56-expressing cells in the control condition, then using the same gate on the transduced cells treated with various compounds to assess % internalization.

Platelet and mast cell purification and activation and 5-HIAA ELISA—Blood from control or treated (Phenelzine or Fluoxetine) mice was drawn from the inferior vena cava into a syringe containing acid citrate dextrose (Sigma Aldrich C3821). Platelet-rich plasma was obtained by mixing blood with modified HEPES-Tyrode's buffer (140mM NaCl, 2mM KCl, 12mM NaHCO3, 0.3mM NaH2PO4, 1mM MgCl2, 5.5 mM glucose, 5mM HEPES, pH6.8) containing 0.35% BSA followed by 300g centrifugation during 4 min. PGI2 was added to platelet-rich plasma (500nM final concentration) and

platelets were then pelleted by centrifugation at 1000g for 6 min. Pelleted platelets were resuspended in modified HEPES-Tyrode's buffer (pH 7.38) containing ADP scavenger apyrase (adenosine-5'-triphosphate diphosphohydrolase, 0.02 IU/ml final) before being put at rest for 45 min at 37°C. Platelets were activated with 0.5 IU/mL of Thrombin for 3 minutes at 37°C, centrifugated and supernatant was collected for further experiments. All reagents were purchased from Sigma, except BSA (RPI research product international). Mast cells were isolated from peritoneal lavage of B6 mice by positive selection (EasySep Mouse CD117 (cKIT) Positive Selection Kit). P815 cells or isolated primary mast cells were diluted in migration medium and seeded in flat 24 well plates (5×10^5 cells / well) 30 min before activation with LPS (100ng/ml, Sigma). Supernatants were collected 2hr after activation, centrifuged at 10000 rpm for 30min at 4°C and tested for migration or ELISA. To quantify 5-HIAA in cell supernatants, Mouse 5-Hydroxyindoleacetic acid (5-HIAA) ELISA Kit (AssayGenie) was used following manufacturer instructions.

Intravital imaging—Intravital imaging of omentum was performed as previously described (Buscher et al., 2016). Briefly, mice were anesthetized with 5% isoflurane (Low-Flow Anesthesia System, Somno Suite®) at 1.5 hr after TG injection. Follow-up surgery and imaging was carried out with lower concentrations of isoflurane (between 0.5% and 0.8%, adjusted according to breathing rate). After removal of abdominal fur, a 1–1.5-cm median incision was done at the linea alba of the upper abdomen to exteriorize the greater omentum, gently handed with cotton-wool tips. A custom-made microscopic stage allowed fixation of the omentum between two cover slips, immersed in warm saline. Throughout the experiment the animals were kept warm on a 37 °C heating pad (Biogenics). To visualize neutrophils and vessels in mixed chimeras, PE-conjugated anti–mouse Ly6G (2ug/200ul, #127608, Biolegend) and dextran Cascade Blue (#D1976, Fisher) were injected i.v. immediately before surgery. For transfer experiments, BM-derived neutrophils were enriched (purity > %80) with negative magnetic selection (EasySep™) following manufacture instructions and using the following biotin-conjugated antibodies: rat anti-mouse anti-CD115 (CSF-IR, #135508), anti-SiglecF (S17007L, #155512), anti-CD3 (145–2C11, #100304, BioLegend), anti-B220 (RA3–6B2, #103204, BioLegend), anti-CD4 (GK1.5, #100404, Biolegend), anti-CD8 (53–6.7, #100704, BioLegend). Purified WT and KO neutrophils were stained with Cell trace Violet or CFSE (#C34554, ThermoFisher), or Deep red (#C34565, Life Tech) according to manufacture instructions and mixed 50:50 before injection (3×10^7 neutrophil / mouse in 200ul saline), 30 min before i.p. TG. Dextran Cascade Blue was used as blood tracer. Pf4Cre mTmG mice expressed GFP selectively in platelets; these mice broadly expressed tdTom in other cell types including neutrophils but the intensity of red fluorescence in these cells was weak as reported(Muzumdar et al., 2007) and was at least 100-fold less intense than for the transferred CMTMR labeled neutrophils such that only the transferred cells were detected. To image inflamed skin, mice were anesthetized with 5% isoflurane at 1.5 hr after *Listeria* ear-pricking. After hair removal, the dorsal side of the ear was attached to a plastic coverslip mounted on a 37°C heating stage. Images were acquired with a Zeiss LSM 7MP equipped with a Chameleon laser (Coherent) and a x20 objective, samples were excited at 820–850nm. For video acquisition, a series of planes of 3μm z-spacing spanning a depth of 30–60 μm were collected every 7–14 s.

Image processing and quantification—Multiphoton intravital movies were imported into IMARIS software (v.9.6.0). Vessel surface was obtained using IMARIS built-in surface function based on dextran-Cascade Blue or dextran-Rhodamine plus CD31-PE or TdTomato (mTmG) signal as indicated. To visualize WT and KO neutrophils in Mrp8-Cre$^+$ mTmG / GPR35 KO mixed chimeras, we injected i.v. anti-Ly6G-PE and imaged 2 independent neutrophil populations: double-positive Mrp8-Cre$^+$ mTmG (GFP$^+$) Ly6G-PE$^+$ WT and single-positive Ly6G-PE$^+$ GPR35 KO neutrophils. To create 2 independent channels for WT and KO neutrophils, GFP channel was subtracted from Ly6G-PE$^+$ channel using channel subtraction function in IMARIS. To track single cells, surface seed points were created and tracked over time with IMARIS spot built-in function. Tracks were manually examined and verified. To quantify transmigrating tracks, an iso-surface of the vessel was generated and tracks that had a shortest distance from the surface of ≤ 0μm (points internal to the surface have a negative value) were selected using Imaris. Of these, tracks that left the vessel and moved at least 5μm away were manually identified and scored as transmigrating. To quantify interactions of WT or KO neutrophils with platelets, iso-surfaces representing WT / KO neutrophils and platelets were created based on channel signal intensity (Imaris). Mean duration contact of WT or KO neutrophils with platelet surfaces was quantified by using Kiss and Run Imaris built-in function. Transmigrating track shortest distance to platelets was automatically quantified after generation of platelets surfaces and tracks (Imaris).

Quantification and Statistical Analysis—Prism software (GraphPad 9.0.1) was used for all statistical analyses. The statistical tests used are specified in the figure legends. Two-tailed unpaired t-tests were performed when comparing only two groups, Paired- t-tests were used to compare internally controlled replicates, and ordinary one-way ANOVA using Turkey's multiple comparisons test was performed when comparing one variable across multiple groups. $P < 0.05$ was considered significant. In summary graphs, points indicate individual samples and horizontal lines are means or medians as indicated. In bar graphs, bars show means and error bars indicate standard error mean (SEM).

Supplementary Material

Refer to Web version on PubMed Central for supplementary material.

Acknowledgements

We thank Serena Ranucci for technical help with Listeria experiments, Jinping An for help with mouse screening, Lihui Duan for help with bioinformatics, Waliul Khan, Huaquing Wang and Francine Cote for Tph1-deficient BM, and Eric Dang and Erick Lu for comments on the manuscript. MDG was supported by an EMBO long-term fellowship and is supported by a CRI Irvington postdoctoral fellowship. JGC is an Investigator of the Howard Hughes Medical Institute. This work was supported by in part by NIH grants R01 AI40098, R01 AI45073 and R01 AI125445.

References:

Agudelo LZ, Ferreira DMS, Cervenka I, Bryzgalova G, Dadvar S, Jannig PR, Pettersson-Klein AT, Lakshmikanth T, Sustarsic EG, Porsmyr-Palmertz M, et al. (2018). Kynurenic Acid and Gpr35 Regulate Adipose Tissue Energy Homeostasis and Inflammation. Cell Metab 27, 378–392 e375. [PubMed: 29414686]

Ajuebor MN, Das AM, Virag L, Flower RJ, Szabo C, and Perretti M. (1999). Role of resident peritoneal macrophages and mast cells in chemokine production and neutrophil migration in acute inflammation: evidence for an inhibitory loop involving endogenous IL-10. J Immunol 162, 1685–1691. [PubMed: 9973430]

Askenase PW, Bursztajn S, Gershon MD, and Gershon RK (1980). T cell-dependent mast cell degranulation and release of serotonin in murine delayed-type hypersensitivity. J Exp Med 152, 1358–1374. [PubMed: 6968811]

Askenase PW, Van Loveren H, Kraeuter-Kops S, Ron Y, Meade R, Theoharides TC, Nordlund JJ, Scovern H, Gerhson MD, and Ptak W. (1983). Defective elicitation of delayed-type hypersensitivity in W/Wv and SI/SId mast cell-deficient mice. J Immunol 131, 2687–2694. [PubMed: 6605986]

Barth MC, Ahluwalia N, Anderson TJ, Hardy GJ, Sinha S, Alvarez-Cardona JA, Pruitt IE, Rhee EP, Colvin RA, and Gerszten RE (2009). Kynurenic acid triggers firm arrest of leukocytes to vascular endothelium under flow conditions. J Biol Chem 284, 19189–19195. [PubMed: 19473985]

Bengel D, Murphy DL, Andrews AM, Wichems CH, Feltner D, Heils A, Mossner R, Westphal H, and Lesch KP (1998). Altered brain serotonin homeostasis and locomotor insensitivity to 3, 4-methylenedioxymethamphetamine ("Ecstasy") in serotonin transporter-deficient mice. Mol Pharmacol 53, 649–655. [PubMed: 9547354]

Berger M, Gray JA, and Roth BL (2009). The expanded biology of serotonin. Annu Rev Med 60, 355–366. [PubMed: 19630576]

Bogoslowski A, Butcher EC, and Kubes P. (2018). Neutrophils recruited through high endothelial venules of the lymph nodes via PNAd intercept disseminating Staphylococcus aureus. Proc Natl Acad Sci U S A 115, 2449–2454. [PubMed: 29378967]

Boleij A, Fathi P, Dalton W, Park B, Wu X, Huso D, Allen J, Besharati S, Anders RA, Housseau F, et al. (2021). G-protein coupled receptor 35 (GPR35) regulates the colonic epithelial cell response to enterotoxigenic Bacteroides fragilis. Commun Biol 4, 585. [PubMed: 33990686]

Bortolato M, Chen K, and Shih JC (2008). Monoamine oxidase inactivation: from pathophysiology to therapeutics. Advanced drug delivery reviews 60, 1527–1533. [PubMed: 18652859]

Bortolato M, Chen K, and Shih JC (2010). The Degradation of Serotonin: Role of MAO. In Handbook of Behavioral Neurobiology of Serotonin, Miller C, and Jacobs B, eds. (Elsevier), pp. 203–218.

Buscher K, Wang H, Zhang X, Striewski P, Wirth B, Saggu G, Lutke-Enking S, Mayadas TN, Ley K, Sorokin L, et al. (2016). Protection from septic peritonitis by rapid neutrophil recruitment through omental high endothelial venules. Nature communications 7, 10828.

Butler A, Hoffman P, Smibert P, Papalexi E, and Satija R. (2018). Integrating single-cell transcriptomic data across different conditions, technologies, and species. Nat Biotechnol 36, 411–420. [PubMed: 29608179]

Callebert J, Esteve JM, Herve P, Peoc'h K, Tournois C, Drouet L, Launay JM, and Maroteaux L. (2006). Evidence for a control of plasma serotonin levels by 5-hydroxytryptamine(2B) receptors in mice. J Pharmacol Exp Ther 317, 724–731. [PubMed: 16461587]

Cheong JE, and Sun L. (2018). Targeting the IDO1/TDO2-KYN-AhR Pathway for Cancer Immunotherapy - Challenges and Opportunities. Trends Pharmacol Sci 39, 307–325. [PubMed: 29254698]

Cloutier N, Pare A, Farndale RW, Schumacher HR, Nigrovic PA, Lacroix S, and Boilard E. (2012). Platelets can enhance vascular permeability. Blood 120, 1334–1343. [PubMed: 22544703]

Cote F, Thevenot E, Fligny C, Fromes Y, Darmon M, Ripoche MA, Bayard E, Hanoun N, Saurini F, Lechat P, et al. (2003). Disruption of the nonneuronal tph1 gene demonstrates the importance of peripheral serotonin in cardiac function. Proc Natl Acad Sci U S A 100, 13525–13530. [PubMed: 14597720]

Deng H, Hu H, and Fang Y. (2012). Multiple tyrosine metabolites are GPR35 agonists. Sci Rep 2, 373. [PubMed: 22523636]

Deppermann C, and Kubes P. (2018). Start a fire, kill the bug: The role of platelets in inflammation and infection. Innate immunity 24, 335–348. [PubMed: 30049243]

Divorty N, Milligan G, Graham D, and Nicklin SA (2018). The Orphan Receptor GPR35 Contributes to Angiotensin II-Induced Hypertension and Cardiac Dysfunction in Mice. Am J Hypertens 31, 1049–1058. [PubMed: 29860395]

Duerschmied D, Suidan GL, Demers M, Herr N, Carbo C, Brill A, Cifuni SM, Mauler M, Cicko S, Bader M, et al. (2013). Platelet serotonin promotes the recruitment of neutrophils to sites of acute inflammation in mice. Blood 121, 1008–1015. [PubMed: 23243271]

Eisa M, Tefera K, and Alvanpour A. (2018). Listeria peritonitis and bacteremia in a patient with cholangiocarcinoma. IDCases 14, e00430.

Enerbäck L. (1963). Serotonin in human mast cells. Nature 197, 610–611.

Etzioni A. (2009). Genetic etiologies of leukocyte adhesion defects. Curr Opin Immunol 21, 481–486. [PubMed: 19647987]

Facciorusso A, Antonino M, Orsitto E, and Sacco R. (2019). Primary and secondary prophylaxis of spontaneous bacterial peritonitis: current state of the art. Expert Rev Gastroenterol Hepatol 13, 751–759. [PubMed: 31304804]

Farooq SM, Hou Y, Li H, O'Meara M, Wang Y, Li C, and Wang JM (2018). Disruption of GPR35 Exacerbates Dextran Sulfate Sodium-Induced Colitis in Mice. Dig Dis Sci 63, 2910–2922. [PubMed: 30043283]

Filippi MD (2019). Neutrophil transendothelial migration: updates and new perspectives. Blood 133, 2149–2158. [PubMed: 30898863]

Foata F, Sprenger N, Rochat F, and Damak S. (2020). Activation of the G-protein coupled receptor GPR35 by human milk oligosaccharides through different pathways. Sci Rep 10, 16117. [PubMed: 32999316]

Freitag A, Wessler I, and Racke K. (1995). Characterization of 5-hydroxytryptamine release from isolated rabbit and rat trachea: the role of neuroendocrine epithelia cells and mast cells. Naunyn Schmiedebergs Arch Pharmacol 353, 55–63. [PubMed: 8750917]

Galli SJ, Gaudenzio N, and Tsai M. (2020). Mast Cells in Inflammation and Disease: Recent Progress and Ongoing Concerns. Annu Rev Immunol 38, 49–77. [PubMed: 32340580]

Gealageas R, Devineau A, So PPL, Kim CMJ, Surendradoss J, Buchwalder C, Heller M, Goebeler V, Dullaghan EM, Grierson DS, et al. (2018). Development of Novel Monoamine Oxidase-B (MAO-B) Inhibitors with Reduced Blood-Brain Barrier Permeability for the Potential Management of Noncentral Nervous System (CNS) Diseases. J Med Chem 61, 7043–7064. [PubMed: 30016860]

Geba GP, Ptak W, Anderson GM, Paliwal V, Ratzlaff RE, Levin J, and Askenase PW (1996). Delayed-type hypersensitivity in mast cell-deficient mice: dependence on platelets for expression of contact sensitivity. J Immunol 157, 557–565. [PubMed: 8752902]

Gershon RK, Askenase PW, and Gershon MD (1975). Requirement for vasoactive amines for production of delayed-type hypersensitvity skin reactions. J Exp Med 142, 732–747. [PubMed: 1165473]

Girbl T, Lenn T, Perez L, Rolas L, Barkaway A, Thiriot A, Del Fresno C, Lynam E, Hub E, Thelen M, et al. (2018). Distinct Compartmentalization of the Chemokines CXCL1 and CXCL2 and the Atypical Receptor ACKR1 Determine Discrete Stages of Neutrophil Diapedesis. Immunity 49, 1062–1076 e1066. [PubMed: 30446388]

Gros A, Syvannarath V, Lamrani L, Ollivier V, Loyau S, Goerge T, Nieswandt B, Jandrot-Perrus M, and Ho-Tin-Noe B. (2015). Single platelets seal neutrophil-induced vascular breaches via GPVI during immune-complex-mediated inflammation in mice. Blood 126, 1017–1026. [PubMed: 26036804]

Herr N, Bode C, and Duerschmied D. (2017). The Effects of Serotonin in Immune Cells. Front Cardiovasc Med 4, 48. [PubMed: 28775986]

Herstowska M, Komorowska O, Cubala WJ, Jakuszkowiak-Wojten K, Galuszko-Wegielnik M, and Landowski J. (2014). Severe skin complications in patients treated with antidepressants: a literature review. Postepy Dermatol Alergol 31, 92–97. [PubMed: 25097474]

Jackson-Jones LH, Smith P, Portman JR, Magalhaes MS, Mylonas KJ, Vermeren MM, Nixon M, Henderson BEP, Dobie R, Vermeren S, et al. (2020). Stromal Cells Covering Omental Fat-Associated Lymphoid Clusters Trigger Formation of Neutrophil Aggregates to Capture Peritoneal Contaminants. Immunity 52, 700–715 e706. [PubMed: 32294409]

Jarchum I, Liu M, Shi C, Equinda M, and Pamer EG (2012). Critical role for MyD88-mediated neutrophil recruitment during Clostridium difficile colitis. Infect Immun 80, 2989–2996. [PubMed: 22689818]

Jenkins L, Alvarez-Curto E, Campbell K, de Munnik S, Canals M, Schlyer S, and Milligan G. (2011). Agonist activation of the G protein-coupled receptor GPR35 involves transmembrane domain III and is transduced via Galpha(1)(3) and beta-arrestin-2. Br J Pharmacol 162, 733–748. [PubMed: 20958291]

Karhausen J, Choi HW, Maddipati KR, Mathew JP, Ma Q, Boulaftali Y, Lee RH, Bergmeier W, and Abraham SN (2020). Platelets trigger perivascular mast cell degranulation to cause inflammatory responses and tissue injury. Sci Adv 6, eaay6314.

Kaya B, Donas C, Wuggenig P, Diaz OE, Morales RA, Melhem H, Swiss IBDCI, Hernandez PP, Kaymak T, Das S, et al. (2020). Lysophosphatidic Acid-Mediated GPR35 Signaling in CX3CR1(+) Macrophages Regulates Intestinal Homeostasis. Cell Rep 32, 107979.

Kornerup KN, Salmon GP, Pitchford SC, Liu WL, and Page CP (2010). Circulating platelet-neutrophil complexes are important for subsequent neutrophil activation and migration. J Appl Physiol (1985) 109, 758–767. [PubMed: 20558756]

Kubes P, and Gaboury JP (1996). Rapid mast cell activation causes leukocyte-dependent and -independent permeability alterations. Am J Physiol 271, H2438–2446. [PubMed: 8997303]

Kushnir-Sukhov NM, Brown JM, Wu Y, Kirshenbaum A, and Metcalfe DD (2007). Human mast cells are capable of serotonin synthesis and release. J Allergy Clin Immunol 119, 498–499. [PubMed: 17291861]

Lefrancais E, Mallavia B, Zhuo H, Calfee CS, and Looney MR (2018). Maladaptive role of neutrophil extracellular traps in pathogen-induced lung injury. JCI Insight 3.

Lefrancais E, Ortiz-Munoz G, Caudrillier A, Mallavia B, Liu F, Sayah DM, Thornton EE, Headley MB, David T, Coughlin SR, et al. (2017). The lung is a site of platelet biogenesis and a reservoir for haematopoietic progenitors. Nature 544, 105–109. [PubMed: 28329764]

Lehtosalo JI, Uusitalo H, Laakso J, Palkama A, and Harkonen M. (1984). Biochemical and immunohistochemical determination of 5-hydroxytryptamine located in mast cells in the trigeminal ganglion of the rat and guinea pig. Histochemistry 80, 219–223. [PubMed: 6202661]

Lindstrom M, Tohmola N, Renkonen R, Hamalainen E, Schalin-Jantti C, and Itkonen O. (2018). Comparison of serum serotonin and serum 5-HIAA LC-MS/MS assays in the diagnosis of serotonin producing neuroendocrine neoplasms: A pilot study. Clin Chim Acta 482, 78–83. [PubMed: 29596816]

Lu E, Wolfreys FD, Muppidi JR, Xu Y, and Cyster JG (2019). S-Geranylgeranyl-L-glutathione is a ligand for human B cell-confinement receptor P2RY8. Nature 567, 244–248. [PubMed: 30842656]

Maas SL, Soehnlein O, and Viola JR (2018). Organ-Specific Mechanisms of Transendothelial Neutrophil Migration in the Lung, Liver, Kidney, and Aorta. Front Immunol 9, 2739. [PubMed: 30538702]

Mackenzie AE, Quon T, Lin LC, Hauser AS, Jenkins L, Inoue A, Tobin AB, Gloriam DE, Hudson BD, and Milligan G. (2019). Receptor selectivity between the G proteins Galpha12 and Galpha13 is defined by a single leucine-to-isoleucine variation. FASEB J 33, 5005–5017. [PubMed: 30601679]

Manne BK, Denorme F, Middleton EA, Portier I, Rowley JW, Stubben C, Petrey AC, Tolley ND, Guo L, Cody M, et al. (2020). Platelet gene expression and function in patients with COVID-19. Blood 136, 1317–1329. [PubMed: 32573711]

Meixiong J, Anderson M, Limjunyawong N, Sabbagh MF, Hu E, Mack MR, Oetjen LK, Wang F, Kim BS, and Dong X. (2019). Activation of Mast-Cell-Expressed Mas-Related G-Protein-Coupled Receptors Drives Non-histaminergic Itch. Immunity 50, 1163–1171 e1165. [PubMed: 31027996]

Morishima T. (1970). 5-hydroxytryptamine (serotonin) and 5-hydroxytryptophan in mast cells of human mastocytosis. Tohoku J Exp Med 102, 121–126. [PubMed: 5312770]

Musgrave T, Benson C, Wong G, Browne I, Tenorio G, Rauw G, Baker GB, and Kerr BJ (2011). The MAO inhibitor phenelzine improves functional outcomes in mice with experimental autoimmune encephalomyelitis (EAE). Brain Behav Immun 25, 1677–1688. [PubMed: 21723939]

Muzumdar MD, Tasic B, Miyamichi K, Li L, and Luo L. (2007). A global double-fluorescent Cre reporter mouse. Genesis 45, 593–605. [PubMed: 17868096]

Nourshargh S, and Alon R. (2014). Leukocyte migration into inflamed tissues. Immunity 41, 694–707. [PubMed: 25517612]

Nowak EC, de Vries VC, Wasiuk A, Ahonen C, Bennett KA, Le Mercier I, Ha DG, and Noelle RJ (2012). Tryptophan hydroxylase-1 regulates immune tolerance and inflammation. J Exp Med 209, 2127–2135. [PubMed: 23008335]

Ohshiro H, Tonai-Kachi H, and Ichikawa K. (2008). GPR35 is a functional receptor in rat dorsal root ganglion neurons. Biochem Biophys Res Commun 365, 344–348. [PubMed: 17996730]

Oka S, Ota R, Shima M, Yamashita A, and Sugiura T. (2010). GPR35 is a novel lysophosphatidic acid receptor. Biochem Biophys Res Commun 395, 232–237. [PubMed: 20361937]

Pagano E, Elias JE, Schneditz G, Saveljeva S, Holland LM, Borrelli F, Karlsen TH, Kaser A, and Kaneider NC (2021). Activation of the GPR35 pathway drives angiogenesis in the tumour microenvironment. Gut.

Page C, and Pitchford S. (2013). Neutrophil and platelet complexes and their relevance to neutrophil recruitment and activation. Int Immunopharmacol 17, 1176–1184. [PubMed: 23810443]

Park SJ, Lee SJ, Nam SY, and Im DS (2018). GPR35 mediates lodoxamide-induced migration inhibitory response but not CXCL17-induced migration stimulatory response in THP-1 cells; is GPR35 a receptor for CXCL17? Br J Pharmacol 175, 154–161. [PubMed: 29068046]

Pietraszek MH, Takahashi S, Takada Y, Ohara K, Inatomi H, Kondo N, Ohara K, and Takada A. (1991). Diurnal patterns of serotonin, 5-hydroxyindoleacetic acid, tryptophan and fibrinolytic activity in blood of depressive patients and healthy volunteers. Thromb Res 64, 243–252. [PubMed: 1725834]

Pletscher A. (1968). Metabolism, transfer and storage of 5-hydroxytryptamine in blood platelets. Br J Pharmacol Chemother 32, 1–16. [PubMed: 4870578]

Plum T, Wang X, Rettel M, Krijgsveld J, Feyerabend TB, and Rodewald HR (2020). Human Mast Cell Proteome Reveals Unique Lineage, Putative Functions, and Structural Basis for Cell Ablation. Immunity 52, 404–416 e405. [PubMed: 32049054]

Poulsen HB, T AS, Bjorkman JT, and Gaini S. (2018). Peritonitis with Listeria monocytogenes in a patient on automated peritoneal dialysis. BMJ Case Rep 2018.

Quon T, Lin LC, Ganguly A, Tobin AB, and Milligan G. (2020). Therapeutic Opportunities and Challenges in Targeting the Orphan G Protein-Coupled Receptor GPR35. ACS Pharmacol Transl Sci 3, 801–812. [PubMed: 33073184]

Rogers MA, Greene MT, Young VB, Saint S, Langa KM, Kao JY, and Aronoff DM (2013). Depression, antidepressant medications, and risk of Clostridium difficile infection. BMC Med 11, 121. [PubMed: 23647647]

Rossaint J, Kuhne K, Skupski J, Van Aken H, Looney MR, Hidalgo A, and Zarbock A. (2016). Directed transport of neutrophil-derived extracellular vesicles enables platelet-mediated innate immune response. Nature communications 7, 13464.

Rosser EC, Piper CJM, Matei DE, Blair PA, Rendeiro AF, Orford M, Alber DG, Krausgruber T, Catalan D, Klein N, et al. (2020). Microbiota-Derived Metabolites Suppress Arthritis by Amplifying Aryl-Hydrocarbon Receptor Activation in Regulatory B Cells. Cell Metab 31, 837–851 e810. [PubMed: 32213346]

Sano H, Suzuki Y, Yazaki R, Tamefusa K, Ohara K, Yokoyama T, Miyasato K, and Ohara K. (1993). Circadian variation in plasma 5-hydroxyindoleacetic acid level during and after alcohol withdrawal: phase advances in alcoholic patients compared with normal subjects. Acta Psychiatr Scand 87, 291–296. [PubMed: 7683838]

Schmid T, Snoek LB, Frohli E, van der Bent ML, Kammenga J, and Hajnal A. (2015). Systemic Regulation of RAS/MAPK Signaling by the Serotonin Metabolite 5-HIAA. PLoS Genet 11, e1005236.

Schneditz G, Elias JE, Pagano E, Zaeem Cader M, Saveljeva S, Long K, Mukhopadhyay S, Arasteh M, Lawley TD, Dougan G, et al. (2019). GPR35 promotes glycolysis, proliferation, and oncogenic signaling by engaging with the sodium potassium pump. Sci Signal 12.

Schwartz JT, Bandyopadhyay S, Kobayashi SD, McCracken J, Whitney AR, Deleo FR, and Allen LA (2013). Francisella tularensis alters human neutrophil gene expression: insights into the molecular basis of delayed neutrophil apoptosis. Journal of innate immunity 5, 124–136. [PubMed: 22986450]

Schwartz LB (1987). Mediators of human mast cells and human mast cell subsets. Ann Allergy 58, 226–235. [PubMed: 3105366]

Shad KF, and Saeed SA (2007). The metabolism of serotonin in neuronal cells in culture and platelets. Exp Brain Res 183, 411–416. [PubMed: 17912506]

Sjoerdsma A, Waalkes TP, and Weissbach H. (1957). Serotonin and histamine in mast cells. Science 125, 1202–1203. [PubMed: 13432786]

Slaba I, and Kubes P. (2017). Platelets and Immunity. In Platelets in Thrombotic and Non-Thrombotic Disorders: Pathophysiology, Pharmacology and Therapeutics: an Update, Gresele P, Kleiman NS, Lopez JA, and Page CP, eds. (Cham: Springer International Publishing), pp. 489–512.

Slaba I, Wang J, Kolaczkowska E, McDonald B, Lee WY, and Kubes P. (2015). Imaging the dynamic platelet-neutrophil response in sterile liver injury and repair in mice. Hepatology 62, 1593–1605. [PubMed: 26202541]

Sonoda H, Aoki J, Hiramatsu T, Ishida M, Bandoh K, Nagai Y, Taguchi R, Inoue K, and Arai H. (2002). A novel phosphatidic acid-selective phospholipase A1 that produces lysophosphatidic acid. J Biol Chem 277, 34254–34263. [PubMed: 12063250]

Strydom N, and Rankin SM (2013). Regulation of circulating neutrophil numbers under homeostasis and in disease. Journal of innate immunity 5, 304–314. [PubMed: 23571274]

Tablang MV (2008). Spontaneous Bacterial Peritonitis Caused by Infection with Listeria monocytogenes. Case Rep Gastroenterol 2, 321–325. [PubMed: 21490863]

Tanaka T, Mori M, Sekino M, Higashijima U, Takaki M, Yamashita Y, Kakiuchi S, Tashiro M, Morimoto K, Tasaki O, et al. (2021). Impact of plasma 5-hydroxyindoleacetic acid, a serotonin metabolite, on clinical outcome in septic shock, and its effect on vascular permeability. Sci Rep 11, 14146. [PubMed: 34238999]

Taniguchi Y, Tonai-Kachi H, and Shinjo K. (2006). Zaprinast, a well-known cyclic guanosine monophosphate-specific phosphodiesterase inhibitor, is an agonist for GPR35. FEBS Lett 580, 5003–5008. [PubMed: 16934253]

Theoharides TC, Bondy PK, Tsakalos ND, and Askenase PW (1982). Differential release of serotonin and histamine from mast cells. Nature 297, 229–231. [PubMed: 6176873]

Tohmola N, Itkonen O, Sane T, Markkanen H, Joenvaara S, Renkonen R, and Hamalainen E. (2014). Analytical and preanalytical validation of a new mass spectrometric serum 5-hydroxyindoleacetic acid assay as neuroendocrine tumor marker. Clin Chim Acta 428, 38–43. [PubMed: 24211728]

Tsukahara T, Hamouda N, Utsumi D, Matsumoto K, Amagase K, and Kato S. (2017). G protein-coupled receptor 35 contributes to mucosal repair in mice via migration of colonic epithelial cells. Pharmacol Res 123, 27–39. [PubMed: 28648739]

Wang J, Simonavicius N, Wu X, Swaminath G, Reagan J, Tian H, and Ling L. (2006). Kynurenic acid as a ligand for orphan G protein-coupled receptor GPR35. J Biol Chem 281, 22021–22028. [PubMed: 16754668]

Wernersson S, and Pejler G. (2014). Mast cell secretory granules: armed for battle. Nat Rev Immunol 14, 478–494. [PubMed: 24903914]

Wirthgen E, Hoeflich A, Rebl A, and Gunther J. (2018). Kynurenic Acid: The Janus-Faced Role of an Immunomodulatory Tryptophan Metabolite and Its Link to Pathological Conditions. Front Immunol 8, 1957. [PubMed: 29379504]

Xie X, Shi Q, Wu P, Zhang X, Kambara H, Su J, Yu H, Park SY, Guo R, Ren Q, et al. (2020). Single-cell transcriptome profiling reveals neutrophil heterogeneity in homeostasis and infection. Nat Immunol 21, 1119–1133. [PubMed: 32719519]

Yabut JM, Desjardins EM, Chan EJ, Day EA, Leroux JM, Wang B, Crane ED, Wong W, Morrison KM, Crane JD, et al. (2020). Genetic deletion of mast cell serotonin synthesis prevents the development of obesity and insulin resistance. Nature communications 11, 463.

Zarbock A, Singbartl K, and Ley K. (2006). Complete reversal of acid-induced acute lung injury by blocking of platelet-neutrophil aggregation. J Clin Invest 116, 3211–3219. [PubMed: 17143330]

Zhao P, Sharir H, Kapur A, Cowan A, Geller EB, Adler MW, Seltzman HH, Reggio PH, Heynen-Genel S, Sauer M, et al. (2010). Targeting of the orphan receptor GPR35 by pamoic acid: a potent activator of extracellular signal-regulated kinase and beta-arrestin2 with antinociceptive activity. Mol Pharmacol 78, 560–568. [PubMed: 20826425]

Highlights

- GPR35 upregulation on activated neutrophils helps in inflammatory recruitment
- Serotonin metabolite 5-hydroxyindoleacetic acid (5-HIAA) acts as a GPR35 ligand
- Platelet- and mast cell-derived 5-HIAA promote neutrophil transendothelial migration
- Inhibitors of serotonin reuptake and metabolism diminish GPR35 function

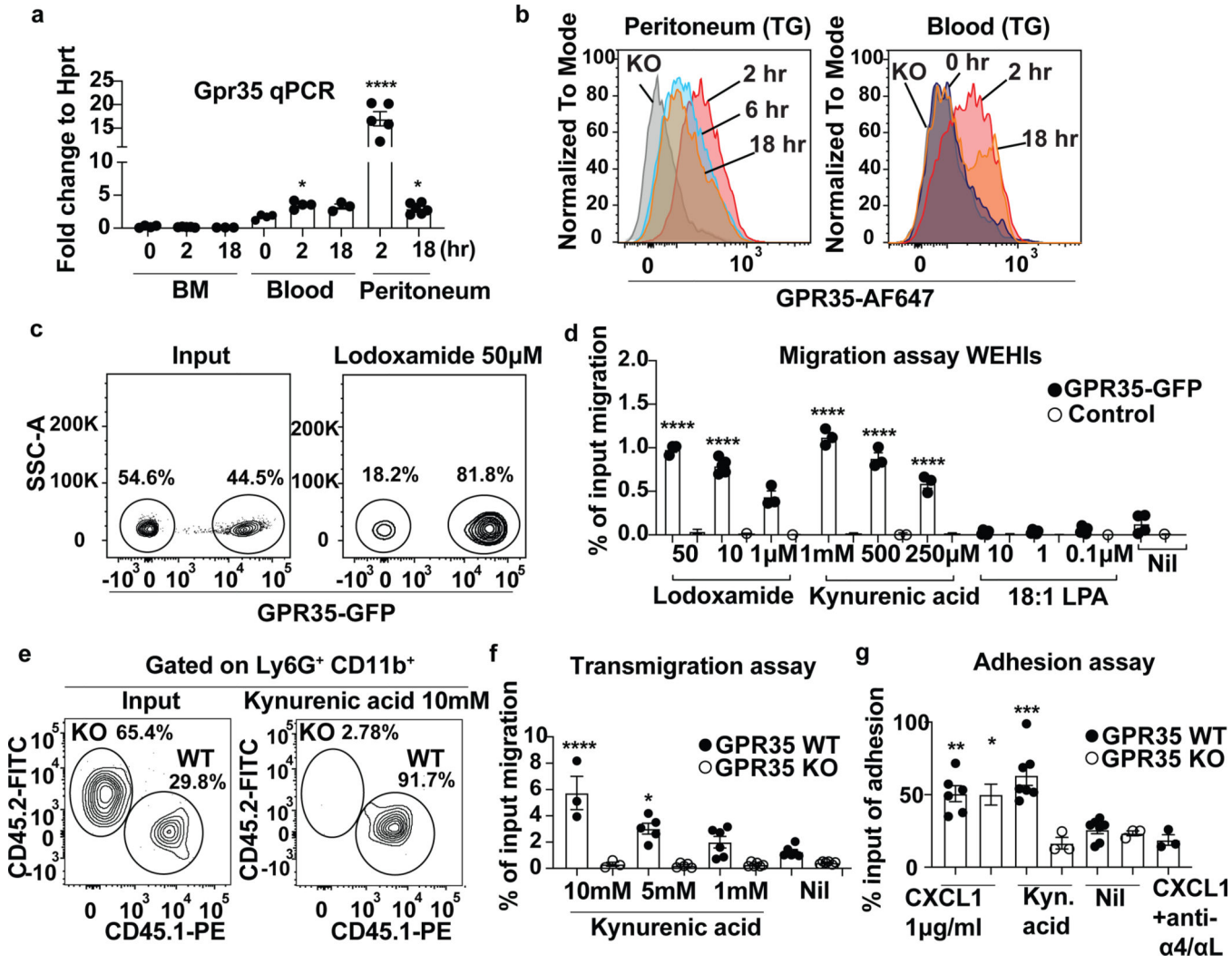

Figure 1. GPR35 is a neutrophil chemotactic receptor.

a, qPCR for expression of Gpr35 (relative to Hprt) in Ly6G$^+$ Ly6C$^+$ CD11b$^+$ CXCR2$^+$ neutrophils sorted from BM (0hr, *n*=4; 2hr *n*=5; 18hr, *n*=3), blood (0hr, *n*=4; 2hr, *n*=4; 18hr, *n*=3) or peritoneum (2hr, *n*=5; 18hr, *n*=6) at indicated time points after TG injection. **b**, Intracellular flow cytometry for GPR35 in Ly6G$^+$ CD11b$^+$ Ly6C$^+$ neutrophils from peritoneum (left) or blood (right) at indicated time points after TG. **c**, Representative flow cytometry plots of GPR35-GFP and control WEHI-231 cells migrating to 50 μM lodoxamide compared to input. **d**, Quantification of transwell migration assays of GPR35-GFP (black) or control (white) WEHI-231 cells to lodoxamide, KynA or 18:1 LPA at the indicated concentrations (*n*=3–6). **e-f**, Representative flow cytometry plots (**e**) and quantification (**f**) of transmigration assay with GPR35 WT (CD45.1) or KO (CD45.2) peritoneal neutrophils 2hr after TG, migrating to KynA at indicated concentrations (*n*=3–6). **g**, Quantification of adhesion assays performed with GPR35 WT or KO peritoneal neutrophils 2hr after TG. Data are pooled from at least 2 independent experiments. Statistics in **a**, **d**, **f** and **g** show comparison of all samples to BM 0hr (**a**) or Nil (**d,f** and **g**). P* < 0.05, **P < 0.005, ***P < 0.001, ****P < 0.0001. See also Figures S1.

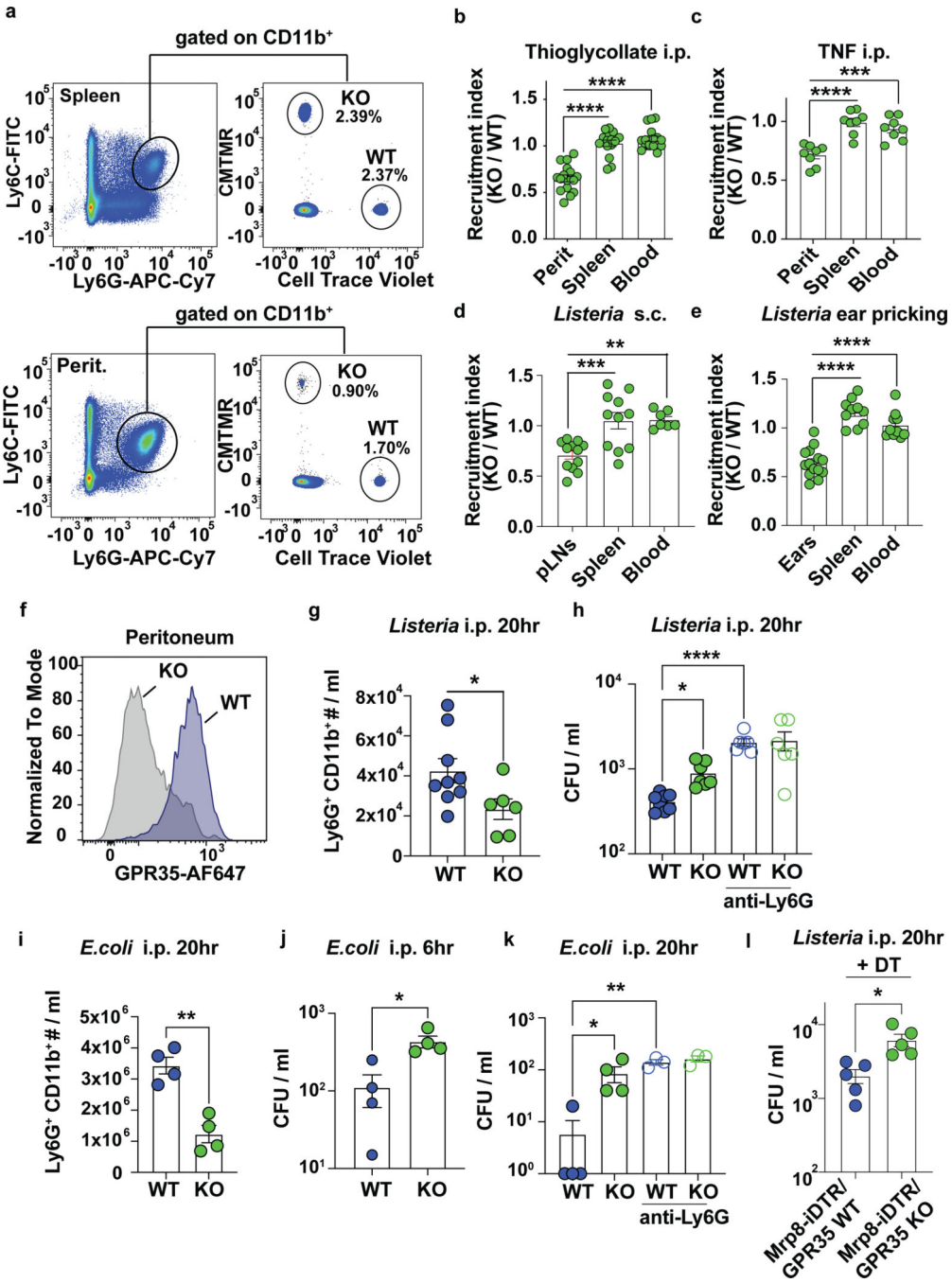

Figure 2. GPR35 sustains neutrophil recruitment to inflamed tissues.

a, Representative flow cytometry plots of spleen (top) and peritoneum (bottom) from mice injected with a 50:50 mix of GPR35 WT (Cell trace violet) and GPR35 KO (CMTMR) BM neutrophils, 18hr after i.p. TG treatment. **b**, Graphs showing neutrophil recruitment index (% KO / % WT) of mice exemplified in (**a**) (n=15–16). **c-e,** Quantification of transferred neutrophil recruitment index in mice injected with either i.p. TNF (2hr, n=8) (**c**), s.c. *Listeria* (20hr, n=10) (**d**), or pricked with *Listeria*-contaminated needle (2hr; ears, n=11; spleen, blood, n=7) (**e**). **f,** Intracellular flow cytometry for GPR35 in $Ly6G^+$ $CD11b^+$ $Ly6C^+$

neutrophils from peritoneum of WT or GPR35 KO mice 20hr after *Listeria* injection. **g,** Quantification of endogenous neutrophil numbers 20hr after peritoneal *Listeria* infection (WT, *n*=9; GPR35 KO, *n*=6). **h,** Quantification of *Listeria* peritoneal CFUs (WT, *n*=8; KO, *n*=7) 20hr after i.p. infection in mice treated or not with Ly6G depleting antibody. **i,** Quantification of endogenous neutrophil numbers 20hr after peritoneal *E. coli* infection (*n*=4). **j, k** Quantification of *E.coli* peritoneal CFUs 6hr (**j**, *n*=4) and 20hr (**k**, *n*=4) after i.p. infection in mice treated or not with Ly6G depleting antibody. **l,** Quantification of *Listeria* peritoneal CFUs (*n*=5) in Mrp8-Cre x iDTR/ GPR35 WT or KO mixed chimeras treated with DT, 20hr after *Listeria* infection Data are pooled from at least 2 independent experiments. *P < 0.05, **P < 0.005, ***P < 0.001, **** P<0,0001. See also Figure S2 and S3.

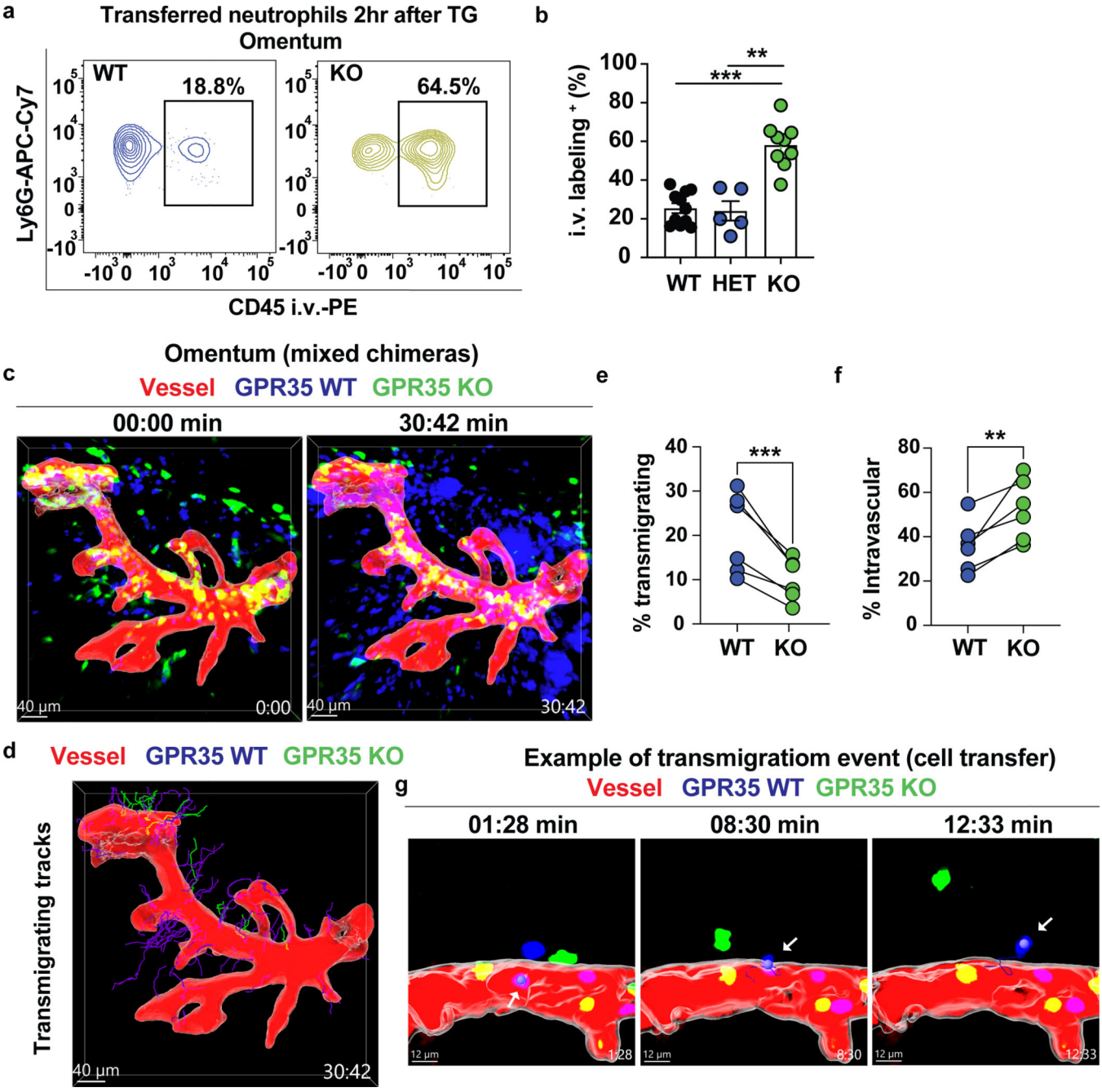

Figure 3. GPR35 supports neutrophil *in vivo* transendothelial migration.

a, Representative flow cytometry plots showing % of CD45-PE^{+} intravascular WT (left) or GPR35 KO (right) transferred neutrophils in the omentum 2hr after i.p. TG. **b**, Quantification of data shown in (**a**) (WT, n=11; HET, n=5; KO, n=9). Data are pooled from 3 independent experiments. **c,** Multiphoton intravital micrographs of Mrp8-Cre^{+} mTmG (blue) and GPR35 KO (green) neutrophils in the omentum of mixed BM chimeric mice injected with labeled dextran to identify vessels (red) and with Ly6G-PE to label neutrophils, 2hr post TG. Time shown in min:sec, See also Movie S1. **d,** Intravital micrograph showing transmigrating (WT blue, KO green) tracks from Movie S1. Image is representative

of at least 3 independent intravital movies. **e**-**f**, Quantification of transmigrating (**e**) or intravascular (**f**) track % of WT or KO neutrophils in the omentum of mice of the type in **c**, 2hr after TG (n=6). **g,** Intravital micrographs of CTV-WT (blue) or CFSE-KO (green) transferred neutrophils in the omentum of mice injected with Dextran-Rhodamine and anti-CD31 PE to identify vessels (red), 2hr post TG (Movie S3). Time shown in min:sec. Arrow highlights transmigrating cell. Data are representative of 4 cell-transfer movies. **P < 0.005, ***P < 0.001. See also Figure S4.

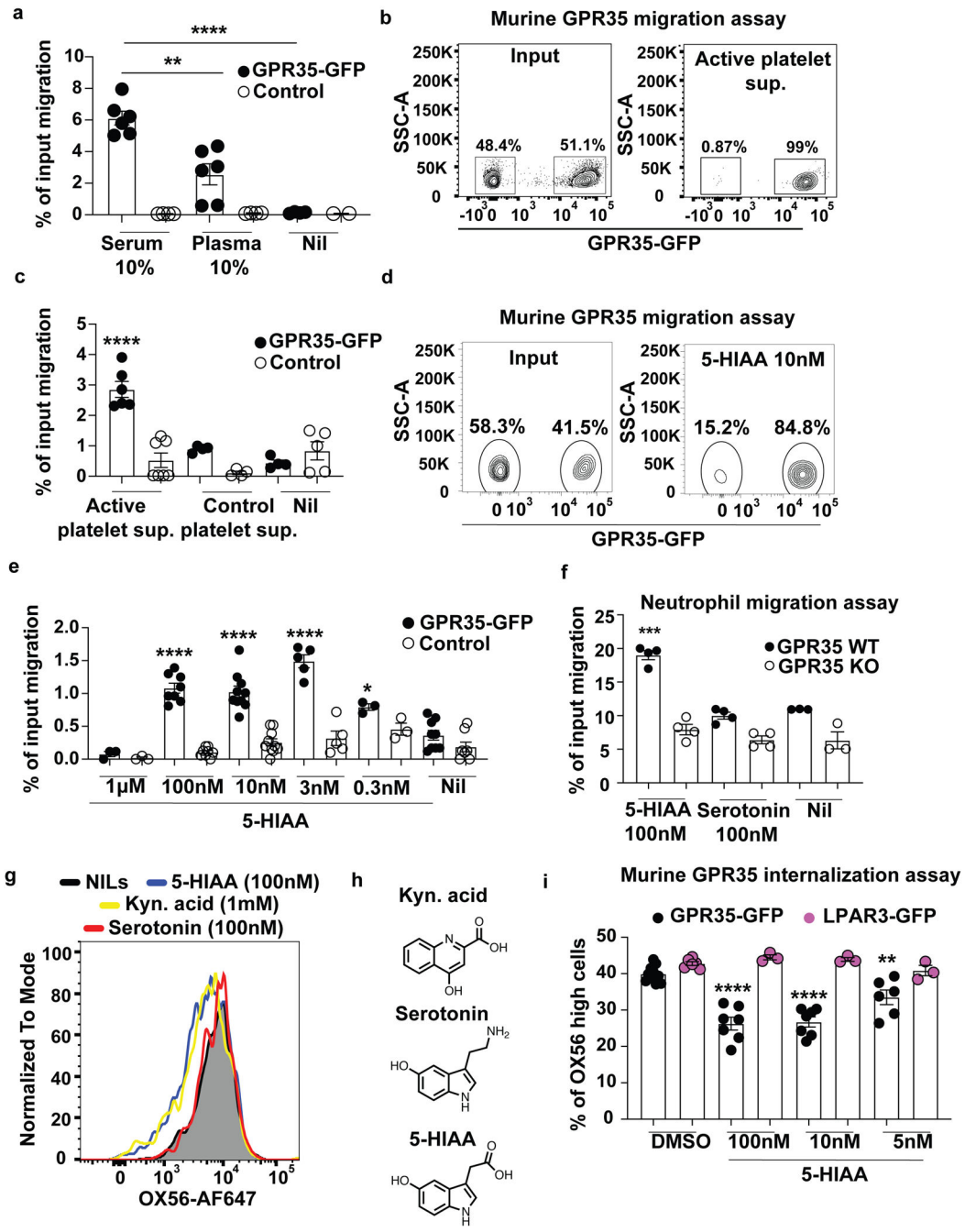

Figure 4. Platelet-derived 5-HIAA is a potent GPR35 ligand

a, Quantification of transwell migration assay of GPR35-GFP or control WEHI-231 cells to 10% serum or plasma (GPR35-GFP: *n*=6; Nil, *n*=4; Control: *n*=5; Nil, *n*=2). Data are pooled from 2 independent experiments. **b-c,** Representative flow cytometry plots (**b**) and quantification (**c**) of GPR35-GFP (black) or control (white) WEHI-231 cells migrating to activated or resting (control) platelet culture supernatants (***n***=4–7). Data are pooled from 3 independent experiments. **d-e,** Representative flow cytometry plots (**d**) and quantification (**e**) of GPR35-GFP and control WEHI-231 transwell migration to 5-HIAA at indicated

concentrations (*n*=3–10). **f,** Quantification of WT or GPR35 KO peritoneal neutrophil (2hr after TG) transwell migration to 100nM 5-HIAA or serotonin (Nil, *n*=3; all others, *n*=4). Data are pooled from 4 (**e**) or 2 (**f**) independent experiments. **g**, Representative flow cytometry histograms of OX56-GPR35 levels in transduced WEHI-231 cells after incubation with 1mM KynA (yellow), 50μM lodoxamide (red), 100nM 5-HIAA (blue) or Nil (black). Image is representative of at least 4 independent experiments. **h**, Diagrams of KynA, serotonin and 5-HIAA molecular structures. **i,** Quantification of OX56 levels in murine OX56-GPR35 and OX56-LPAR3 WEHI-231 cells incubated with 5-HIAA at indicated concentrations (*n*=3–11). Data are pooled from 4 independent experiments. *P<0.05, **P < 0.005, ***P < 0.001, ****P < 0.0001. See also Figure S5.

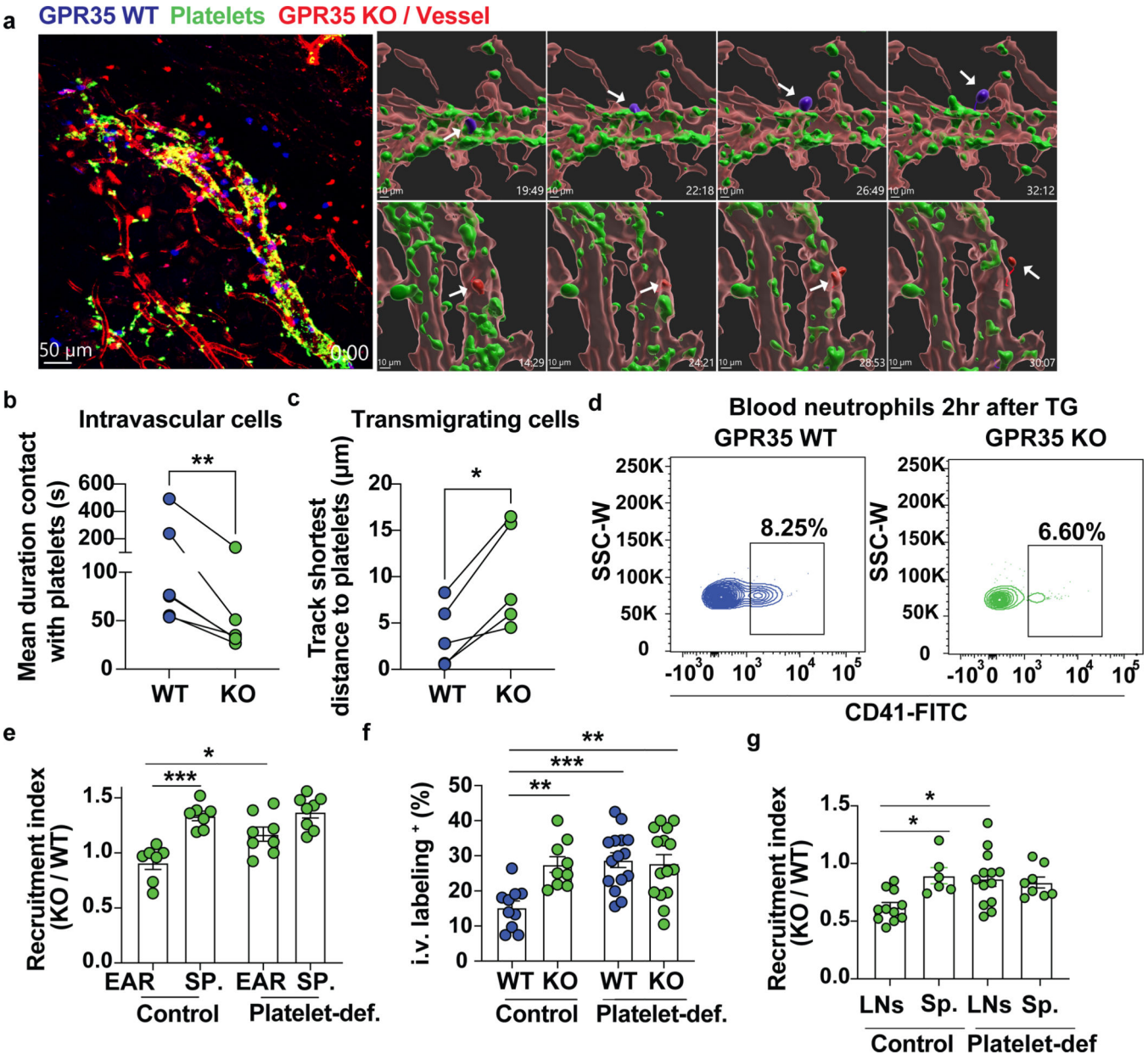

Figure 5. Activated platelets promote GPR35-dependent neutrophil transmigration.

a, Multiphoton intravital micrographs of CTV-WT (blue) or CMTMR-GPR35 KO (red) neutrophils in the omentum of Pf4-Cre x mTmG (platelets GFP$^+$, green) recipients 2hr after TG (see also Movie S5). Vessels identified based on tdTom distribution (red). Images are representative of 3 independent intravital movies. Left: Composite image at time 0. Right: Time series showing example WT (upper) and KO (lower) cells transmigrating (arrow). Endothelium shown as an iso-surface based on tdTom fluorescence. Time stamp shows min:sec. **b-c,** Quantification of mean contact time with platelets (**b**) (n=6) and transmigrating track shortest distances from platelets (**c**) (n=6) of images of the type in (**a**) and Movie S5. Each dot represents individual movies. **d**, Representative flow cytometry plots showing % of CD41$^+$ WT (left) or KO (right) transferred neutrophils in blood 2hr

after TG. **e-f**, Quantification of (**e**) neutrophil recruitment index in WT (n=7) or platelet-deficient (n=8) and (**f**) intravascular neutrophil % in WT (left; WT, n=10; KO, n=9) or platelet-deficient (right; n=15) mice 2hr after *Listeria* skin-pricking. **g,** Quantification of neutrophil recruitment index in LNs and spleen of WT or platelet-deficient mice (n=8–13). Data are pooled from at least 2 independent experiments. *P < 0.05, **P< 0.005, ***P< 0.001. See also Figure S6.

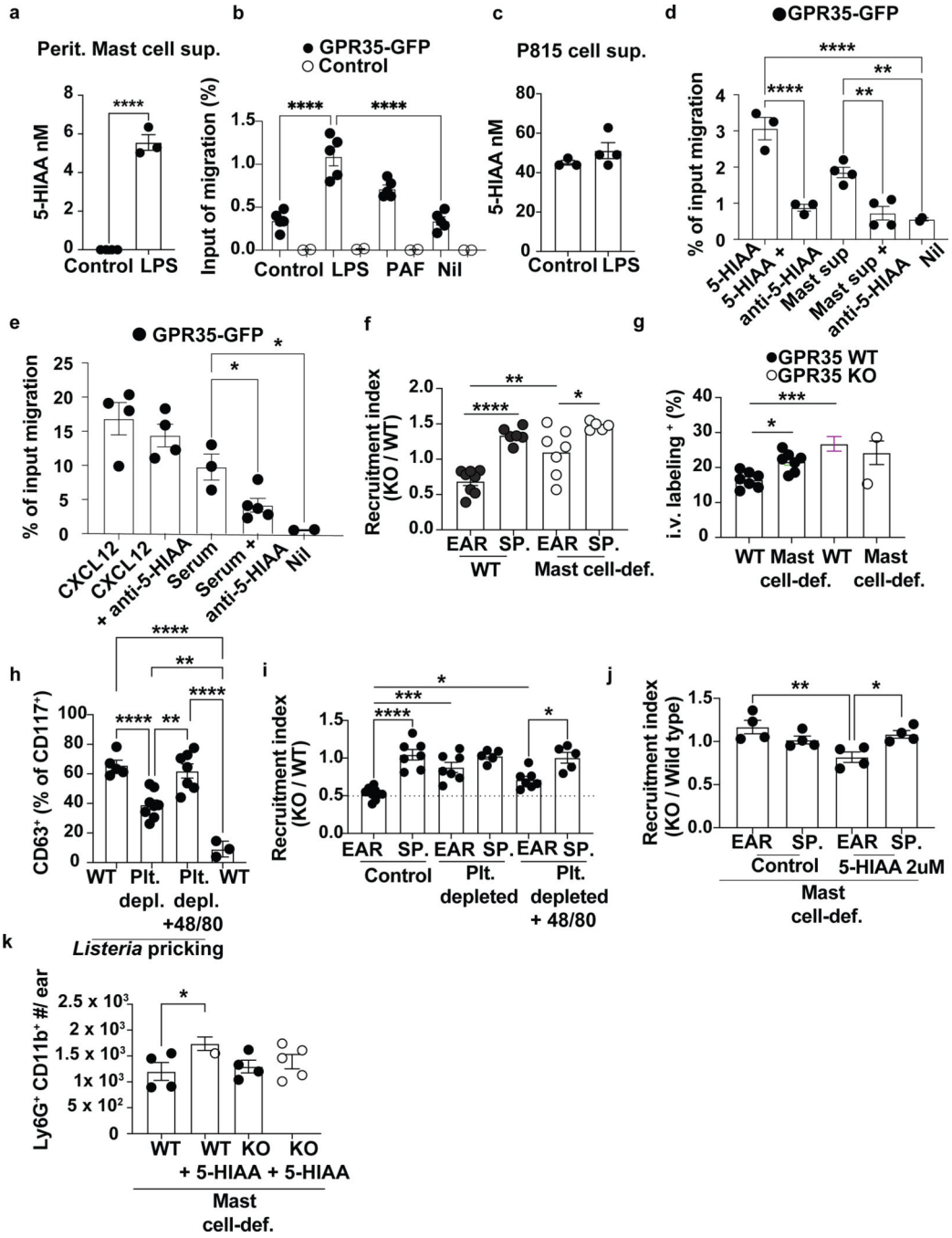

Figure 6. Activated mast cells are sources of 5-HIAA and collaborate with platelets to sustain GPR35-dependent neutrophil recruitment.

a, Graph showing ELISA quantification of 5-HIAA in control (n=4) or LPS-treated (n=3) peritoneal mast cell supernatants. Single dots represent biological replicates. Unpaired t test was applied: ****P < 0.0001. **b**, Quantification of GPR35-GFP WEHI-231 cell migration to control or LPS-treated peritoneal mast cell supernatants (n=5). **c,** Graph showing ELISA quantification of 5-HIAA in control (n=3) or LPS-treated (n=4) P815 mast cell line supernatants. **d, e,** Quantification of GPR35-GFP WEHI-231 cell migration to (**d**)

5-HIAA (5nM), mast cell supernatants (50%),(**e**) CXCL12 (100ng/ml) or serum (5%) with the addition of anti-5-HIAA (2ug/ml) as indicated (n=2–5). **f, g,** Transferred neutrophil recruitment index (n=5–8) (**f**) and i.v. labeling (n=6–7) (**g**) in WT or mast cell-deficient mice 2hr after *Listeria* pricking. **h,** Quantification of $CD63^+$ cells out of total $CD117^+$ mast cells in 2hr *Listeria* pricked skin of control (n=5), platelet-depleted (n=8), platelet-depleted + compound 48/80 s.c. (n=7) or untreated controls (n=3).. **i** Transferred neutrophil recruitment index (n=5–7) in control, platelet-depleted or platelet-depleted and 48/80 treated mice 2hr after *Listeria* pricking. Data pooled from 2 independent experiments. **j, k,** Transferred neutrophil recruitment index (**j**) and numbers (**k**) in mast cell-deficient mice 2hr after *Listeria* skin-pricking and s.c. injection with DMSO (control) or 5-HIAA (n=4). *P < 0.05, **P < 0.005, ***P < 0.001, ****P < 0.0001.

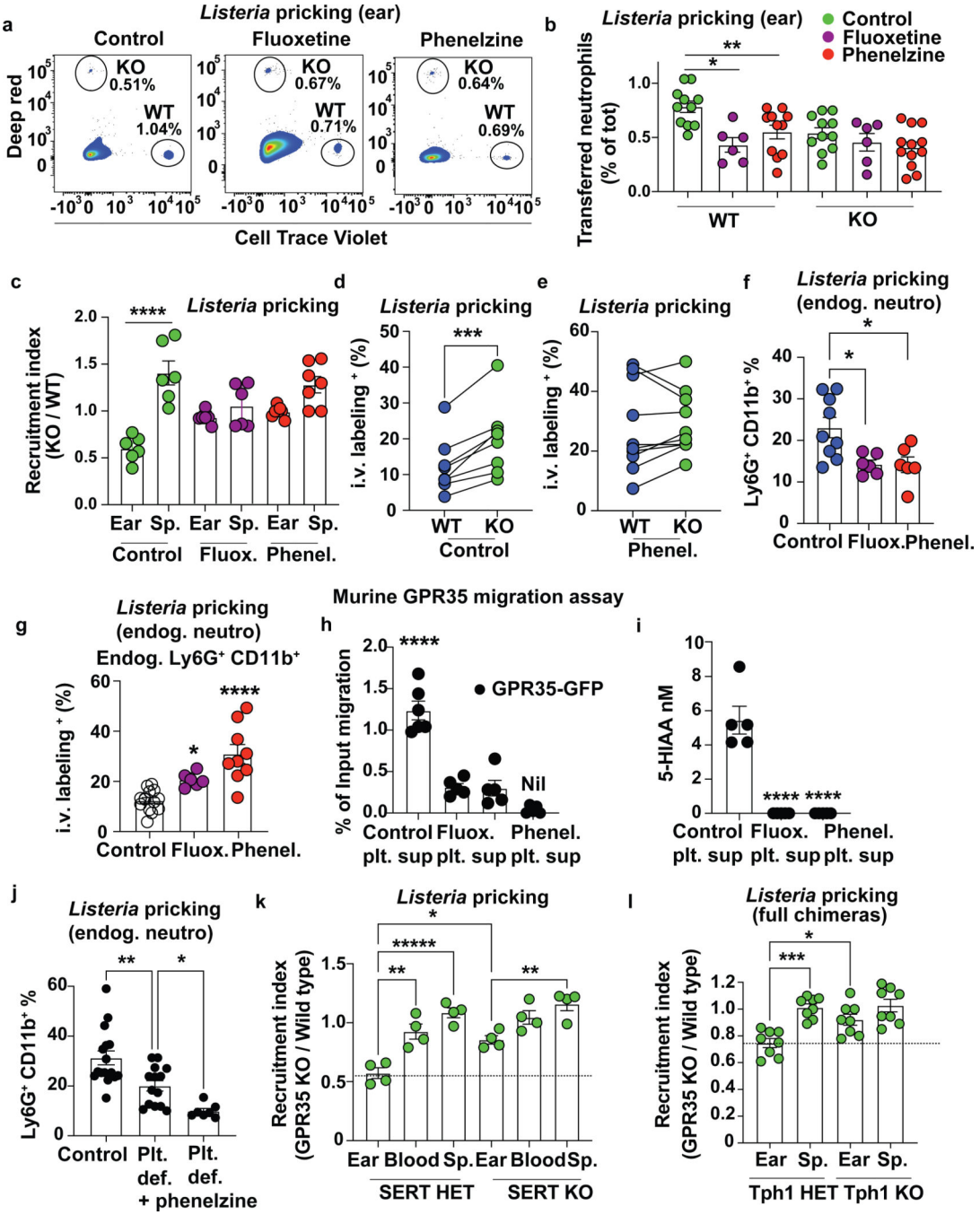

Figure 7. Platelet and mast cell-derived 5-HIAA promote neutrophil recruitment *in vivo*

a-b, Representative flow cytometry plots (**a**) and quantification (**b**) of % transferred WT or KO neutrophils in ear skin of controls (green) or mice pretreated with Fluoxetine (purple) or Phenelzine (red), 2hr after *Listeria* skin-pricking (n=6–12). **c,** Graph showing quantification of transferred neutrophil recruitment index in controls or mice pretreated with Fluoxetine (purple) or Phenelzine (red), 2hr after *Listeria* skin-pricking (n=6–7). Graphs depict bars with mean +/− SEM. **d,** Quantification of CD45-PE^{+} intravascular transferred neutrophils in controls (**d**) and mice treated with Phenelzine (**e**), 2hr after *Listeria* skin-pricking (**b**,

n=8, **c**, *n*=10). **f,g,** Graphs showing quantification of endogenous neutrophil % (**f**) (WT, *n*=9; Phenelzine, *n*=6; Fluoxetine, *n*=6) or CD45-PE^{+} intravascular endogenous neutrophils (**g**) in mice untreated (*n*=14) treated with Phenelzine (red) (*n*=9) or Fluoxetine (purple) (*n*=6). **h**, Quantification of GPR35-GFP WEHI-231 cell migration to activated platelet culture supernatants from mice treated with Phenelzine or Fluoxetine (Control platelet sup., *n*=6; all others, *n*=5). **i,** ELISA quantification of 5-HIAA in supernatants of activated platelets from control, phenelzine-treated or fluoxetine-treated mice. Data are representative of 2 independent experiments. **j,** Quantification of Ly6G^{+} CD11b^{+} endogenous neutrophils in the skin of WT (*n*=16), platelet-deficient (*n*=14) or platelet-deficient mice treated with phenelzine (*n*=7) 2hr after *Listeria* skin-pricking. Data are pooled from at least 3 independent experiments. **k, l,** Transferred neutrophil recruitment index in SERT Het or KO mice (**k,** *n*=4) or Tph1 Het or KO chimeras (**l,** *n*=8) 2hr after *Listeria* skin-pricking. Data are pooled from 2 independent experiments. *P < 0.05, **P < 0.005, ***P<0.001 ****P < 0.0001. See also Figures S7 and S8.

Key Resource table.

REAGENT or RESOURCE	SOURCE	IDENTIFIER
Antibodies		
FITC-conjugated rat anti-mouse Ly6C (AL-21)	BD	#553104
APC-Cy7-conjugated rat anti-mouse Ly6G (1A8)	TONBO	#25–1276-U100
BV785-conjugated rat anti-mouse CD11b (M1/70,	BioLegend	#101243
APC-conjugated rat anti-mouse CXCR2 (SA044G4)	BioLegend	#149312
FITC-conjugated rat anti-mouse CD45.2 antibody (104)	BioLegend	#109805
PE-conjugated rat anti-mouse CD45.1 (A20)	BioLegend	#110708
FITC-conjugated rat anti-mouse CD11a (I21/7)	BioLegend	#153105
Biotin-conjugated rat-anti mouse CD18 (C71/16)	BD	#557439
FITC-conjugated rat anti mouse LFA-1 (REA880)	Miltenyi Biotec	#130–114-422
APC-conjugated rat anti-mouse CXCR2 (SA044G4)	BioLegend	#149311
PE-Cy7-conjugated rat anti-mouse CD62L (Mel-14)	BioLegend	#104418
BV421-conjugated rat anti-mouse PSGL1 (2PH1)	BD	#562807
PE-conjugated rat anti-mouse CD117 (2B8)	Fisher	#553355
FITC-conjugated rat anti-mouse CD63 (NVG-2)	BioLegend	#143920
PE- conjugated anti-mouse CD45.2 (104)	BioLegend	#109808
Biotinylated OX56 antibody	Bio X Cell	#0806–1
AF647-conjugated anti-mouse/rat CD90.1	BioLegend	#202508
Streptavidin–PE	BioLegend	#405203
Rabbit polyclonal anti-mouse GPR35	Biomatik	#2314-AP106RI
AF647-Goat anti-Rabbit IgG (H+L) Highly Cross-Adsorbed Ab	Fisher Scientific	#A21245
FITC- conjugated rat anti-mouse CD41 (MWReg30)	BioLegend	#133903
anti-5-HIAA polyclonal	My-Bio-Source	#MBS2032649
Bacterial and virus strains		
Listeria monocytogenes	A gift from D. Portnoy, UC Berkley	N/A
E.coli (K1)	A gift from Dr. Matthay, UCSF	N/A
Chemicals, peptides, and recombinant proteins		
Lodoxamide	Sigma	#SML2307
Kynurenic acid	Sigma	#K3375
18:1 LPA	Sigma	#L7260
5-HIAA	Sigma	#H8876
Serotonin	Cayman Chemical	#14332
PTX	List Biological Labs, Inc	#181
Diptheria Toxin	Millipore	#322326
Critical commercial assays		
Mouse 5-Hydroxyindoleacetic acid (5HIAA 5-HIAA) ELISA Kit	AssayGenie	# MOEB2528

REAGENT or RESOURCE	SOURCE	IDENTIFIER
Antibodies		
Deposited data		
Murine neutrophil data	Xie et al., 2020	GSE137540
Human neutrophil data	Schwartz et al., 2013	BioGps
Experimental models: Cell lines		
WEHI-231	Cell line was previously obtained from other laboratories and further authentication was not performed.	N/A
bEND3	Cell line was previously obtained from other laboratories and further authentication was not performed.	N/A
HEK293T (Platinum-E (Plat-E) Retroviral Packaging Cell Line)	Gift from S. Schwab, NYU	N/A
Experimental models: Organisms/strains		
C57BL/6J	Jackson Laboratories	#000664
B6.SJL-Ptprca Pepcb/BoyJ	Jackson Laboratories	#002014
Gpr35−/−	EMMA (EM09677; Gpr35tm1b(EUCOMM)Hmgu)	N/A
Pf4-Cre x mTmG (Gt(ROSA)26Sortm4(ACTBtdTomato,-EGFP)Luo/J)	Looney lab, UCSF (Lefrancais et al., 2017)	N/A
Mrp8-Cre x mTmG	Looney lab, UCSF (Lefrancais et al., 2018)	N/A
Kit/v x Kit/W	Jackson Laboratories	#100410
B6.129(Cg)-Slc6a4tm1Kpl/J	Jackson Laboratories	#008355
Tph1 Het and KO Bone Marrow	Waliul Khan lab, McMaster Univ. (Cote et al., 2003)	N/A
Oligonucleotides		
CTGGACGAGTCGGTCAGAAG-Fwd (Gpr35 qPCR)	N/A	N/A
GCGTTGGAAAGATTCGCCTTT-Rev (Gpr35 qPCR)	N/A	N/A
Recombinant DNA		
MSCV-IRES-Thy1.1	Addgene	Plasmid ID: 17442
MSCV-IRES-GFP	Addgene	Plasmid ID: 20672
Software and algorithms		
IMARIS (v.9.6.0)	Imaris softawre	https://imaris.oxinst.com/
Flowjo (v.10.6.2)	Flowjo	https://www.flowjo.com/
Prism (GraphPad 9.0.1)	GraphPad software	https://www.graphpad.com/scientific-software/prism/
Seurat R package (version 2.2)	Seurat	https://satijalab.org/seurat/
R studio (3.5)	R software	https://www.rstudio.com/
Adobe Illustrator CS6	Adobe System	N/A